Selenization of ZIF-67 as Electrode Material for Supercapacitor Application

By

Iqra Shaukat

Reg. No. 00000328955

Session 2020-22

Supervised by

Prof Dr. Naseem Iqbal

US-Pakistan Center for Advanced Studies in Energy (USPCAS-E)

National University of Sciences and Technology (NUST)

H-12, Islamabad 44000, Pakistan

June 2023

Selenization of ZIF-67 as Electrode Material for Supercapacitor Application

By

Iqra Shaukat

Reg. No. 00000328955

Session 2020-22

Supervised by

Dr. Naseem Iqbal

A Thesis Submitted to the US-Pakistan Center for Advanced Studies in Energy in partial fulfillment of the requirements for the degree of

MASTER of SCIENCE in

Energy Systems Engineering

US-Pakistan Center for Advanced Studies in Energy (USPCAS-E)

National University of Sciences and Technology (NUST)

H-12, Islamabad 44000, Pakistan

June 2023

THESIS ACCEPTANCE CERTIFICATE

Certified that the final copy of MS/MPhil thesis written by **Ms. Iqra Shaukat** (Registration No. 00000328955), of US-Pakistan Center for Advanced Studies in Energy (USPCAS-E) has been vetted by undersigned, found complete in all respects as per NUST Statues/Regulations, is within the similarity indices limit and is accepted as partial fulfillment for the award of MS degree. It is further certified that necessary amendments as pointed out by GEC members of the scholar have also been incorporated in the said thesis.

Signature: _____

Name of Supervisor: _____

Date: _____

Signature (HOD): _____

Date: _____

Signature (Dean/Principal): _____

Date: _____

Certificate

This is to certify that work in this thesis has been carried out by **Ms. Iqra Shaukat** and completed under my supervision in Synthesis, Energy Storage laboratory, and Advance Energy Materials Laboratory, US-Pakistan Center for Advanced Studies in Energy (USPCAS-E), National University of Sciences and Technology, H-12, Islamabad, Pakistan.

Supervisor:

_____
Prof. Dr. Naseem Iqbal
USPCAS-E
NUST, Islamabad

GEC member 1:

_____
Dr. Ghulam Ali
USPCAS-E
NUST, Islamabad

GEC member 2:

_____
Dr. Nadia Shehzad
USPCAS-E
NUST, Islamabad

GEC member 3:

_____
Dr. Mustafa Anwar
USPCAS-E
NUST, Islamabad

HOD-ESE:

_____
Dr. Rabia Liaquat
USPCAS-E
NUST, Islamabad

Dean/Principal:

_____
Prof. Dr. Adeel Waqas
USPCAS-E
NUST, Islamabad

Dedication

To my parents, who supported me in every aspect of life, my siblings and friends.

Acknowledgments

First and foremost, I am thankful to **Almighty ALLAH** who is the creator and author of knowledge. Indeed, without YOUR blessings, this task would not have been possible. And I acknowledge that without YOUR willingness and guidance, I would not have done a single task. I am grateful to my parents for their unconditional love and sacrifices. your debt for your encouragement, financial and moral support. Thank you for keeping confidence in me.

Prof. Dr. Naseem Iqbal, I express my sincerest gratitude to you for this opportunity, for your teaching, mentorship, and patience throughout the research. It has been truly a privilege to work with you. I would like to thank my GEC members **Dr. Ghulam Ali, Dr. Mustafa Anwar,** and **Dr. Nadia Shahzad** for their guidance and help throughout my research.

I am also thankful to the staff of Synthesis and Energy Storage Lab, specially **Engineer Naveed Ahmed,** who helped in my research and gave valuable advice during my experimentation. I am also grateful to the other lab staff, faculty members, and administration who were a part of this journey. Also, all my friends, including **Maryam Raza, Rabbia Naz, Rabia Ahmad, Neelam Zaman, and Rimsha Mehek** for their support both academically and in general. And to life, an extraordinary experience with so many things to enjoy within a short span. Thank you for giving me so much in the years past, and for more to discover in the years to come.

Abstract

ZIF-based materials are considered efficient electrodes for supercapacitor applications because of their adjustable structure and greater surface area features. CoSe/NC based composites have recently gained significant attention as high-performance electrode materials for supercapacitor applications. These composites typically consist of CoSe nanoparticles integrated with nitrogen-doped carbon (NC) matrices, which exhibit excellent electrochemical properties such as high specific capacitance, good rate capability, and long-term cycling stability. In this work, CoSe/NC composites were synthesized by using Selenium powder and ZIF-67, ZIF-67 being prepared from co-precipitation method using cobalt nitrate hexahydrate and 2- methyl imidazolate, the purple-colored precipitates of ZIF-67 obtained at the end of reaction were then grounded after that,by keeping the mass ratio of ZIF-67 constant and the amount of Selenium powder is varied, pyrolyzed at 800 ℃ under a reducing atmosphere(Ar /H_2) for 4 hours, XRD was done for all the three prepared electrodes showing the successful formation of CoSe .SEM analysis showed nanoporous morphologies of CoSe composites of all the prepared samples annealed at 800 °C . The highest degree of graphitization in the case of CoSe-1 could be assigned to better electrochemical performance. The CoSe-1 showed excellent electrochemical performance with the highest value of specific capacitance (746F g^{-1}at 2mVs^{-1}), showing a rate capability of 82.3% after 4000 cycles because of optimize ratio of Cobalt and selenium in CoSe-1**.** Overall, CoSe/NC based composites CoSe-1 showed a promising avenue for the development of high-performance electrode materials for supercapacitor applications.

Keywords: Transition Metal Selenides, Cobalt Metal-organic Framework, Selenium powder, Zeolitic Imidazolate Framework, Nanoporous carbon, Cobalt Selenide

Table of Contents

List of Figures

List of Tables

List of Publication

Title: Selenization of ZIF-67 as Electrode Material for Supercapacitor Application

Authors: Iqra Shaukat, Dr. Naseem Iqbal, Tayyaba Noor, Maryam Raza, Rabia Ahmad

Status: Under Review (Electrochemica Acta)

Introduction

1.1 Supercapacitors

Supercapacitors represent a class of energy storage devices that exhibit the ability to quickly store and release energy, rendering them a promising substitute to conventional batteries. These devices have garnered considerable attention in recent times, primarily due to their impressive attributes such as high-power density, rapid charging capacity, extended cycle life, and minimal self-discharge rates. The electrochemical mechanism of super capacitors involves the accumulation of energy through an electrostatic field, wherein the device comprises of two electrodes, a separator, and an electrolyte. The electrodes, usually composed of activated carbon or high-surface-area materials, furnish a large surface area for the electrostatic charge to accumulate. The separator is a thin film that allows ions to permeate while keeping the electrodes from touching, whereas the electrolyte conducts ions between the electrodes. One of the critical benefits of supercapacitors over traditional batteries is their ability to recharge and discharge swiftly, with batteries typically taking hours to charge while supercapacitors can accomplish it in seconds or minutes. Moreover, supercapacitors offer a longer cycle life than batteries, implying they can be charged and discharged numerous times before deterioration. This quality makes them an economical and environmentally-friendly solution for specific applications, such as energy storage for electric vehicles. As research and development progress in this domain, supercapacitors have the potential to transform energy storage and contribute towards a sustainable future [1].

1.2 Background

In recent years, a promising technology for energy storage called supercapacitors or ultracapacitors has emerged. The origins of supercapacitors can be traced back to the early 1950s when researchers first identified the phenomenon of double-layer capacitance, which involves the accumulation of charge at the interface between an electrode with a high surface area and an electrolyte.

Supercapacitors made their first commercial appearance as backup power supplies for static random-access memory (SRAM) in the 1980s. Over time, they have been utilized in a variety of applications, such as regenerative braking systems in hybrid electric vehicles, grid-scale energy storage, and peak power management in renewable energy systems.

Supercapacitors offer a significant advantage in their ability to rapidly store and release energy. Their capacity to charge and discharge in a matter of seconds makes them highly beneficial for applications that demand quick response times and high power densities. Compared to batteries, supercapacitors have a longer cycle life, which means they can undergo many more charge and discharge cycles before deteriorating. Nonetheless, their energy density is still lower than that of conventional batteries, which limits their use in certain areas. Nevertheless, there is ongoing research and development focused on enhancing the energy density of supercapacitors and lowering their cost to make them more competitive with traditional energy storage technologies [2].

As a whole, supercapacitors exhibit considerable potential as an energy storage technology and could be applied across a variety of industries. Ongoing advancements in research suggest that supercapacitors will play a vital role in meeting the world's increasing energy requirements in a sustainable and cost-effective manner [3].

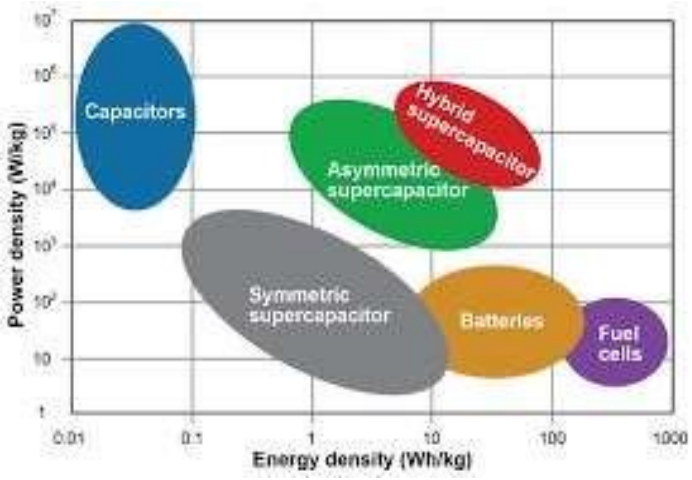

Figure 1.1. Ragone plot showing (Specific energy vs Specific power) [4].

Depending on how they store energy, supercapacitors fall into two categories.

1.2.1 Electrical double layer capacitor (EDLC)

EDLC, or Electric Double-Layer Capacitor, is a type of supercapacitor that stores electrical energy via charge separation at the interface between an electrode and an electrolyte. This differs from traditional capacitors which store energy in an electric field between two conductive plates. EDLC supercapacitors use high surface area electrodes coated with a porous material, creating a larger interface area between the electrode and electrolyte. However, EDLC supercapacitors have limitations including lower energy density compared to batteries and self-discharge over time. Researchers are currently working to improve energy density and reduce self-discharge, potentially leading to broader applications in the future [5].

1.2.2 Pseudocapacitors

Pseudocapacitors are a unique type of electrochemical capacitor that store energy using reversible faradaic redox reactions, in addition to the non-faradaic charge storage mechanisms of conventional capacitors. The reversible electron transfer between the electrode and electrolyte creates an electrical double layer and/or a solid-state pseudocapacitive material on the electrode surface. Pseudocapacitors have several advantages over traditional capacitors and EDLC supercapacitors, including higher energy density and better long-term stability. They are often composed of transition metal oxides and/or conducting polymers, which have high specific capacitance due to their pseudocapacitive behavior. Pseudocapacitors have a broad range of applications, including energy storage systems, hybrid electric vehicles, and portable electronics. They are especially useful in situations requiring high power and energy density[5]. Working of a supercapacitors.

1.3 Working of a supercapacitors

Energy storage can be classified into two types: EDLC and pseudocapacitors. These types operate on different chemistry principles. While EDLC stores electrostatic charge on the electrode surface, pseudocapacitors use other electrochemical processes.

1.3.1 Working Mechanism Pseudocapacitor

Pseudocapacitor electrodes are constructed from materials with high pseudocapacitance, which describes a material's ability to store and release electrical charge through redox reactions. These materials include transition metal oxides, conducting polymers, and other high specific capacitance materials. The electrolyte employed in pseudocapacitors is typically an aqueous or organic solution that contains ions capable of engaging in redox reactions at the electrode surface. When voltage is applied to a pseudocapacitor, charge separation takes place at the electrode-electrolyte interface. This results in the formation of a solid-state pseudocapacitive material on the surface of the electrode that stores electrical charge. The charge accumulated in the pseudocapacitive material can be released quickly, providing high power output [6].

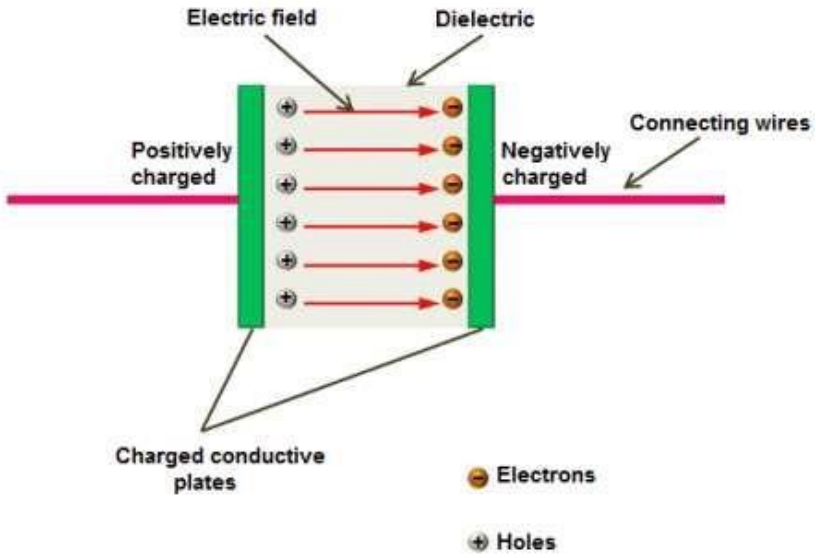

Figure 1.2. Construction of a simple capacitor [7].

In a conventional capacitor, electrical charge is stored in the strong electric field between two conductive plates that are separated by an insulating material, as shown in Figure 1.2. Due to their small plate area and restricted separation distance, traditional electrostatic capacitors can only store a limited amount of energy. However, supercapacitors that operate on the EDL mechanism are capable of storing considerably more energy owing to their enormous interfacial area and atomic charge separation distance. Stern built upon the earlier research by Helmholtz and Chapman on the EDL mechanism and developed and refined it in the 1920s.

The Stern model identified two separate regions of ion distribution, namely the inner compact layer and the outer diffuse layer, as illustrated in Figure 1.3. The compact layer is where hydrous ions are firmly adsorbed by the electrode. The compact layer is made up of specific ions in the interior Helmholtz plane (IHP) and nonspecific counter ions in the exterior Helmholtz plane (OHP). In addition, due to the movement of electrolyte ions in the solution, an electrolyte diffuse layer develops around an electrode [8].

In equation (1) C_{dl} is EDL capacitance, C_H is compact capacitance and C_{diff} is diffusion capacitance.

$$\frac{1}{C_{dl}} = \frac{1}{C_H} + \frac{1}{C_{diff}} \quad (1)$$

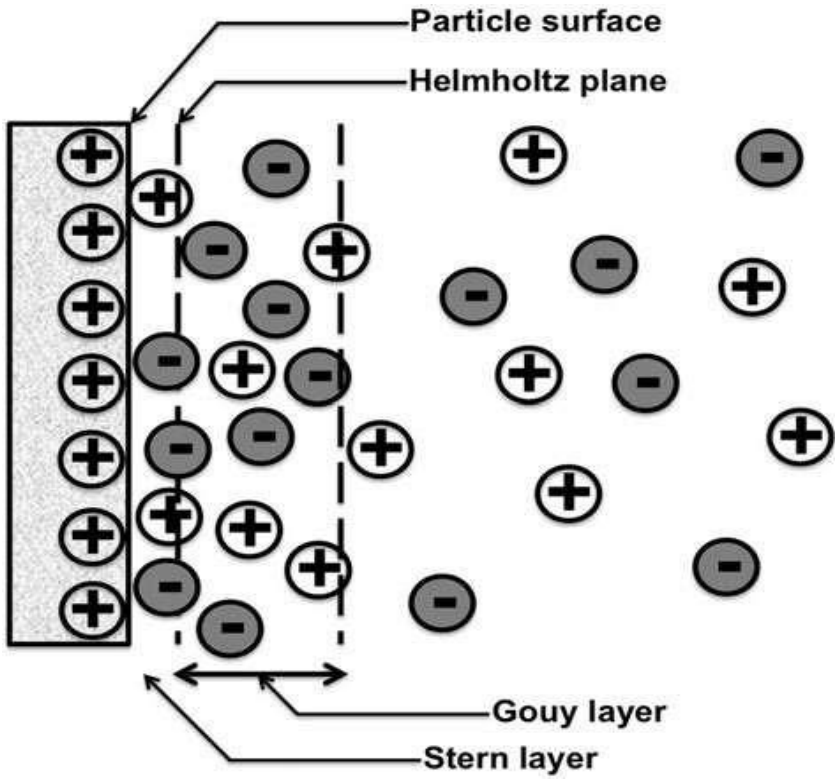

Figure 1.3. Helmholtz Plane and Gouy Layer in Stern model [9].

Thermodynamically induced pseudocapacitance is distinct from EDL capacitance. Redox faradic reactions occur on the electrode materials of a pseudocapacitor, allowing for charge to be transferred across the electrode/electrolyte interface. Unlike EDL capacitors, pseudocapacitors' processes are influenced by a thermodynamic potential difference during charge accumulation, making them more reversible and more powerful. Faradaic processes occur in three different ways at pseudocapacitive electrodes.

- Adsorption of H^+ from the electrolyte that is reversible in nature.
- Ions from the electrolyte are involved in redox reactions.
- Conducting polymer-based electrodes with reversible doping and deducing processes [10].

1.3.1 Working Mechanism of EDLC

In the two-plate EDLC capacitor, the charging accumulator is located at the electrode-to-electrolyte contact point (as shown in Figure 1.4). During charging, electrons move from the negative electrode to the positive electrode through the external circuit. It is not entirely clear why cations and anions in the electrolyte are attracted to the negative and positive electrodes, respectively. During discharge, two opposing forces are at work: electrons and ions. Unlike in pseudocapacitors (shown in Figure 1.4), no redox reaction occurs in EDLCs, and charges are not transferred between the two layers. Due to the lower power density of Faradaic systems, the power density of EDLCs may be lower than that of pseudocapacitors. However, pseudocapacitors have a larger specific capacity and energy density than EDLCs because they are a Faradaic device.

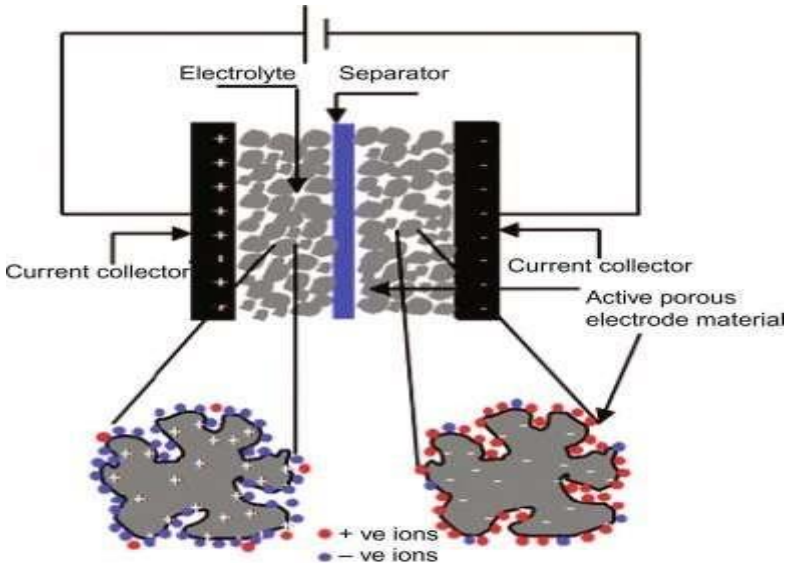

Figure 1.4. Representation of EDLC (high surface area porous electrode is used) [11].

Figure 1.4 illustrates how voltage is applied to the capacitor causing opposing charges to be collected on each electrode, which creates an eclectic field that lets the capacitor store energy. The capacitance of a system, C, may be written as:

$$C = \frac{Q}{V}$$

Q stands for the stored charges, while V stands for the applied voltage. The capacitance C is governed by the electrode surface area and inversely proportional to the electrode's distance. Hence, capacitance can be as:

$$C = \varepsilon_o \varepsilon_r \frac{Q}{V}$$

ε_r is the isolating substance between the electrodes, and ε_o is the dielectric constant, always with relative permittivity. Using The output of a supercapacitor is determined by its energy and power density, which can be calculated using equations (1) and (2). The power density of a supercapacitor increases with its charge processing. When electrodes and electrolytes come into contact, electrostatic interactions are generated by the electric double layers (EDLs). The capacitance of a supercapacitor is determined by the charge on the electrode surface. Redox reactions typically involve an EDL capacitance component that is related to the electrochemically active interface area. Active species commonly used in supercapacitors include carbon surfaces with functional groups, organic polymers such as Polypyrrole (PPy), and transition metal oxides like nickel, iron, and manganese. Pseudocapacitors can achieve very high energy density when multiple oxidation states of the electrode materials can be attained, resulting in capacitance that is 10 to 100 times greater than EDLC. However, their sluggish faradic reactions and morphological changes during operation lead to lower specific power and decreased life expectancy [12].

1.4 Supercapacitors Performance Optimization

Maximizing specific capacitance in supercapacitors requires careful consideration of electrode pore size. Three types of pore sizes, micropores, mesopores, and macropores, can be found within the electrode material. Micropores are particularly important for the adsorption and retention of ions within the double layer, while mesopores and macropores are necessary to allow for rapid ion movement throughout the material. The accessibility of these pores to the electrolyte is crucial to the performance of supercapacitors. The choice of electrode material also plays a significant role, and researchers are continuously exploring new materials like graphene, metal oxides, and conducting polymers that offer high specific capacitance, low resistance, and long cycle life. The choice of electrolyte and operating conditions can also affect performance, with the most conductive electrolyte salt and optimizing voltage range and charging/discharging rate improving power density. Combining supercapacitors with other energy storage technologies, such as batteries or fuel cells, can lead to improved overall energy storage performance by leveraging the high

power density of supercapacitors and the high energy density of batteries or fuel cells. [13].

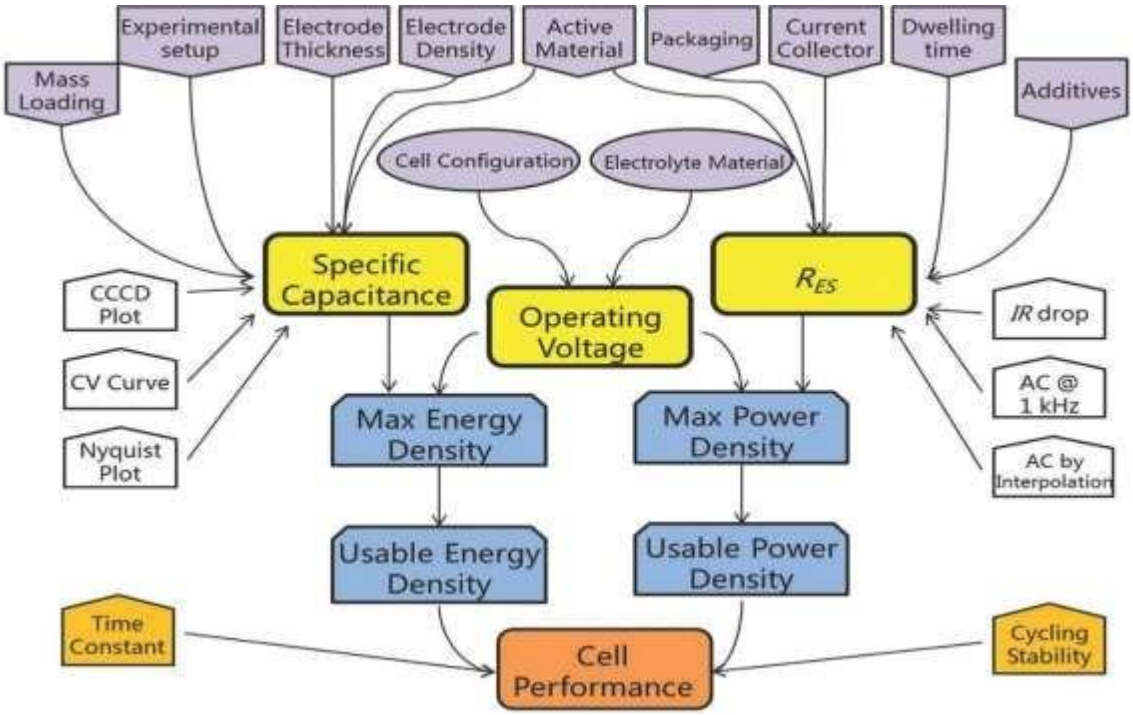

Figure 1.5. Performance Optimization of Supercapacitors [14].

1.5 Problem Statement

The large effective surface area, high porosity, and multiple redox reaction sites of MOF-based materials make them highly attractive for use in electrochemical devices. Despite these benefits, pure MOFs have certain limitations, such as low conductivity and particulate aggregation, which hinder their effectiveness as electrode materials. As a result, supercapacitors that use MOFs as electrodes typically have low energy densities, often less than 50Wh/kg, whereas batteries have energy densities ranging from 30-300Wh/kg. Additionally, cyclic stability is a significant concern when utilizing MOFs as electrode materials.

1.6 Objectives

The aim of this research was to produce a porous electrode material with a high specific capacitance. To study the physicochemical properties, X-ray diffraction (XRD), scanning electron microscopy (SEM), transmission electron microscopy (TEM), X-ray photoelectron spectroscopy (XPS) were employed. The electrochemical properties were

analyzed using techniques such as electrochemical impedance spectroscopy (EIS), cyclic voltammetry (CV), galvanostatic charge-discharge (GCD) and cyclic stability test for 10,000 cycles. It was found that the specific capacity of a carbon-based supercapacitor is significantly influenced by the surface area and the presence of defects.

1.7 Summary

This chapter discuss the background and comparison of all energy storage systems and compare them to supercapacitors. Further chapter 1 discusses the types and working of supercapacitors and their performance evaluation in detail.

List of References

1 Sinha, P. and K.K. Kar, *Introduction to supercapacitors*, in *Handbook of Nanocomposite Supercapacitor Materials II: Performance*. 2020, Springer. p. 1- 28.

2. Samantara, A.K. and S. Ratha, *Materials development for Active/Passive components of a supercapacitor: background, present status and futureperspective.* 2017.

3. Samantara, A.K., et al., *Historical background and present status of the supercapacitors.* Materials development for active/passive components of a supercapacitor: background, present status and future perspective, 2018: p. 9-10.

4. Wayu, M., *Manganese oxide carbon-based nanocomposite in energy storage applications.* Solids, 2021. **2**(2): p. 232-248.

5. Lakal, N., S. Dubal, and P. Lokhande, *Supercapacitors: An introduction.*

Nanotechnology in the Automotive Industry, 2022: p. 459-466.

6. Bhojane, P., *Recent advances and fundamentals of Pseudocapacitors: Materials, mechanism, and its understanding.* Journal of Energy Storage, 2022. **45**: p.103654.

7. Saleem, A.M., V. Desmaris, and P. Enoksson, *Performance enhancement of carbon nanomaterials for supercapacitors.* Journal of Nanomaterials, 2016. **2016**.

8. Jadhav, V.V., et al., *Electrochemical supercapacitors: history, types, designing processes, operation mechanisms, and advantages and disadvantages.* Bismuth- Ferrite-Based Electrochemical Supercapacitors, 2020: p. 11-36.

9. Piacenza, E., A. Presentato, and R.J. Turner, *Stability of biogenic metal (loid) nanomaterials related to the colloidal stabilization theory of chemical nanostructures.* Critical reviews in biotechnology, 2018. **38**(8): p. 1137-1156.

10. Khot, M. and A. Kiani, *A review on the advances in electrochemical capacitive charge storage in transition metal oxide electrodes for pseudocapacitors.* International Journal of Energy Research, 2022.

11. Yin, L., et al., *Ionic liquid electrolytes in electric double layer capacitors.* Sci. China Mater, 2019. **62**(11): p. 1537-1555.

12. Najib, S. and E. Erdem, *Current progress achieved in novel materials for supercapacitor electrodes: mini review.* Nanoscale Advances, 2019. **1**(8): p. 2817-2827.
13. Wu, S., et al., *A review of performance optimization of MOF-derived metal oxide as electrode materials for supercapacitors.* International Journal of Energy Research, 2019. **43**(2): p. 697-716.
14. Zhang, S. and N. Pan, *Supercapacitors performance evaluation.* Advanced Energy Materials, 2015. **5**(6): p. 1401401.
15. Gou, Q., et al., *Recent advances on boosting the cell voltage of aqueous supercapacitors.* Nano-Micro Letters, 2020. **12**: p. 1-22.
16. Jänes, A., H. Kurig, and E. Lust, *Characterisation of activated nanoporous carbon for supercapacitor electrode materials.* Carbon, 2007. **45**(6): p. 1226-1233.
17 Zhu, C., et al., *All metal nitrides solid-state asymmetric supercapacitors.* Materials, 2015. **27**(31): p. 4566-4571.

Chapter 2: Literature Review

2.1 Electrode Materials

The charge storage and final capacitance of a supercapacitor are significantly influenced by the selection of electrode materials. In order to achieve optimal capacitance, it is essential to consider the effective surface area and electrical conductivity of the electrode material. Carbon-based materials like graphite, graphene, carbon nanotubes, and activated carbon are popular choices due to their capacity to store charge through electrical double-layer capacitance on their surface. To attain high capacitance levels, the material must have a high surface area, suitable pore size and distribution, and functional groups. Additionally, other materials such as metal oxides, conducting polymers, metal-organic frameworks, black phosphorus, M Xenes, and metal nitrides are also suitable for use as super capacitor electrode materials[18].Several key properties are necessary for electrode materials to ensure optimal performance. First and foremost, they should possess a high surface area to provide ample sites for charge storage. In addition, good electrical conductivity is crucial to guarantee efficient charge transfer between the electrode and the electrolyte. The pore size of the electrode material also affects its performance, with an appropriate pore size allowing for better ion diffusion and charge transfer. Uniform pore size distribution is also vital to ensure uniform electrolyte penetration, leading to improved performance. The presence of functional groups, particularly oxygen-containing groups, enhances the electrode material's electrochemical performance. Furthermore, the electrode material must be chemically stable in the electrolyte to prevent degradation and loss of performance over time. Finally, the cost and abundance of the electrode material are important considerations as they affect the overall cost of the supercapacitor device and its mass production[19].

2.2 Categories of Electrode Materials

The classification of electrode materials for supercapacitors can be broadly divided into two categories: carbon-based materials and pseudocapacitive materials.

Due to their high surface area and excellent electrical conductivity, carbon-based materials like activated carbon, graphite, graphene, and carbon nanotubes are the most widely utilized electrode materials for supercapacitors. These materials store charge by accumulating ions at the electrode-electrolyte interface through the electrical double-layer capacitance (EDLC) mechanism.

In contrast to carbon-based materials, pseudocapacitive materials accumulate charge through surface redox reactions, which encompass the reversible transfer of electrons between the electrode and the electrolyte. Despite usually having a lower surface area than carbon-based materials, pseudocapacitive materials can attain higher capacitance since they can store charge via both the EDLC and pseudocapacitance mechanisms. Metal oxides, conducting polymers, and transition metal dichalcogenides are some examples of pseudocapacitive materials.

Hybrid materials are an additional classification of electrode materials for supercapacitors that integrate the characteristics of both carbon-based and pseudocapacitive materials. By doing so, they can provide the advantages of high capacitance and high power density. Carbon nanotube-metal oxide composites, graphene-metal oxide composites, and conducting polymer-metal oxide composites are some instances of hybrid materials.

The selection of the electrode material is determined by the particular application and the intended performance features of the super capacitor.

Metal-organic frameworks (MOFs) are a kind of porous materials that are constructed from metal ions or clusters connected by organic ligands to form a three-dimensional structure. These MOFs possess a large surface area, adjustable pore size, and a broad spectrum of functional groups that make them attractive for different purposes, including gas storage, sensing, and catalysis. Recently, MOFs have also garnered considerable interest as possible electrode materials for energy storage devices like batteries and supercapacitors. Depending on the metal ion and ligand utilized, MOFs can store charge via various mechanisms, such as redox reactions, double-layer capacitance, and pseudocapacitance. They have demonstrated remarkable electrochemical performance with high capacitance, rapid charge-discharge rates, and favorable cycling stability. However, the limited conductivity of MOFs is a significant obstacle that may constrain their charge transfer kinetics and overall electrochemical performance in practical

applications. Several methods such as hybridization with conductive materials, structural modification, and doping have been proposed to enhance the conductivity of MOFs. All things considered, MOFs are a promising class of materials for energy storage applications, and their distinctive properties and versatility are continuing to attract interest from the scientific community [20].

2.3 Carbon based composites

Carbon-based materials consist mainly of carbon atoms and have diverse properties and applications, including their use as electrode materials in supercapacitors. These materials are particularly appealing due to their low cost, abundance, and excellent electrochemical properties. They store charge through the electrical double-layer capacitance (EDLC) mechanism, where ions accumulate at the electrode-electrolyte interface, and can also display pseudocapacitive behavior through surface redox reactions. To optimize their performance for specific applications, various modifications and combinations of carbon-based materials have been proposed [21].

2.3.1 Activated Carbon (AC)

Activated carbon is a widely used carbon-based material for supercapacitor electrodes, owing to its high surface area and exceptional electrical conductivity. It is produced by heating carbon-rich materials, such as coconut shells, wood, or coal, in the presence of a gas or activating agent at high temperatures. The resulting surface of the carbon develops a network of pores, which offer a significant surface area for effective ion transport and charge storage. Activated carbon's properties can be tailored by adjusting the raw material and activation parameters, such as temperature, duration, and type of activating agent. This allows for the production of activated carbons with customized characteristics for specific applications. However, activated carbon may suffer from limited capacitance and poor stability at high voltages, which can restrict its performance in certain applications. Several modifications and combinations of activated carbon with other materials have been proposed to overcome these limitations and enhance its electrochemical performance. [22].

2.3.2 Carbon nano tubes (CNTs)

Carbon nanotubes (CNTs) are synthesized through sp^2 hybridization, where graphene sheets are wrapped in covalently bonded carbon atoms. Graphene sheets, on the other hand, are classified based on the number of layers and porosity, and provide mechanical strength and conductivity to the composite material. A supercapacitor electrode with a CNT-doped composite exhibited minimal capacitance fading after 50,000 cycles in aqueous electrolyte solutions. In contrast, a similar system without CNTs was unable to match its performance and experienced a decrease in capacitance after 30,000 cycles, as shown in (Figure 2.1) [6]. In Comparison to the combination of CNTs and GQDs, the composites performed better with a capacitance of 200 mF/cm2 compared to 0.44 mF/cm^2.Despite its fascinating properties, graphene is still not a practical option for electrode materials in energy storage devices, as demonstrated by this study.

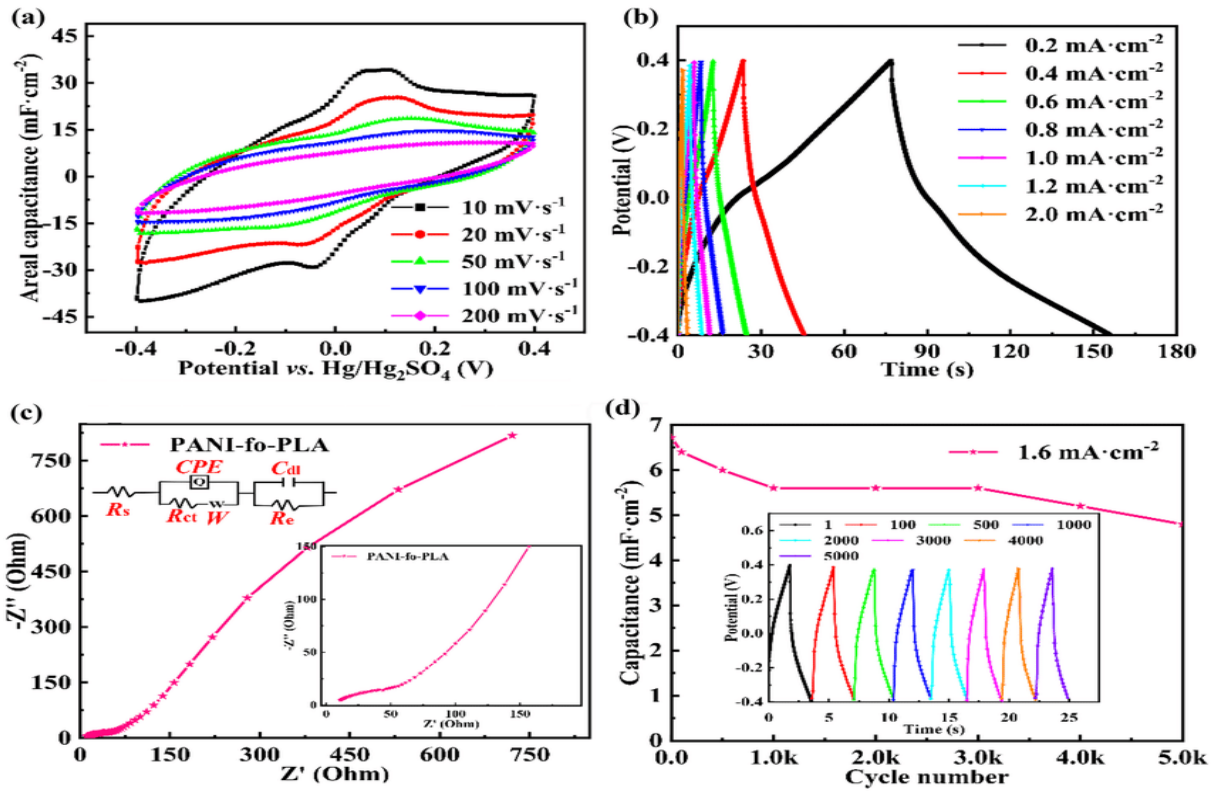

Figure 2.1. (a, b, c, f) Cyclic voltammetry, gravimetric Charge/Discharge and Nyquist plot of carbon-based polymer electrodesin 3M KOH electrolyte (d) Carbon based polymer electrode with CNTs (e) Capacity vs. cycle number plot [23]

The addition of carbon nanotubes (CNTs) to the $CuCo_2S_4$ matrix resulted in numerous pathways for efficient electron transfer and ion diffusion, leading to a significant improvement in the faradaic reactions of the $CuCo_2S_4$ electrode during energy storage. Specifically, at 1A g^{-1}, the $CuCo_2S_4$/CNTs-3.2% electrode demonstrated a specific capacitance of 557.5 F g^{-1}, which was notably higher than the pristine $CuCo_2S_4$ electrode with 373.4 F g^{-1} and the CuO/Co_3O_4/CNTs-3.2% electrode with 356.5 F g^{-1}. An asymmetric supercapacitor (ASC) was then constructed to assess its energy storage potential, with the $CuCo_2S_4$/CNTs-3.2% electrode serving as the positive electrode and active carbon as the negative electrode. At a power density of 402.7 W kg^{-1}, the ASC exhibited an energy density of 23.2 Wh kg^{-1}. Furthermore, the residual specific capacitance of the ASC device remained at 85.7% of its original value even after 10,000 cycles, indicating remarkable cycle stability [24].

A simple technique for producing large-scale, self-supporting film electrodes composed of $NiCo_2O_4$@carbon nanotube (CNT) composites for supercapacitors has been presented by Wu et al. The $NiCo_2O_4$@CNT/CNT film electrodes were fabricated by vacuum filtering stacked $NiCo_2O_4$@CNT and CNT alternately. Of all the composite electrodes synthesized, the one fired in air demonstrated the best electrochemical performance, exhibiting a specific capacitance of 1,590 F g^{-1} at 0.5 A g^{-1} with outstanding stability. These lightweight, flexible, and self-standing film electrodes, which were approximately 24.3 μm thick, also displayed a high volumetric capacitance of 873 F cm^{-3} at 0.5 A g^{-1}. To evaluate the practicality of these electrodes, an all-solid-state asymmetric supercapacitor was created, which included a composite film electrode with a treated carbon cloth electrode. This supercapacitor not only achieved a high energy density of roughly 27.6 Wh kg^{-1} at 0.55 kW kg^{-1} but also exhibited excellent cycling stability, maintaining around 95% of its original capacitance after 5000 cycles [25].

2.3.3 N-doped carbons

Carbon materials can undergo physical, chemical, and electrochemical changes through nitrogen doping. Nitric acid can modify the crystallographic and electronic arrangement of carbons, increasing chemical stability and improving electrical conduction. Nitrogen-doped carbons are utilized not only in supercapacitors and catalysis but also in adsorption and separation processes. Most Nitrogen-doped carbon materials are created using N-

containing precursors, with the amount of nitrogen matter in the precursors serving as a limiting factor for this type of synthesis. Attempts to increase the nitrogen quantity in the precursors have resulted in the degradation of the carbons' mesostructure. A recent report indicates that carbonization, nitrogen functionalization, and activation can be combined into a single process to synthesize N-doped materials. [26].

The incorporation of ultrafine zeolitic imidazolate framework (ZIF-8) nanoparticles into electrospun polyacrylonitrile (PAN) is followed by carbonization to produce hierarchical porous nanofibers made up of interconnected nitrogen-doped carbon hollow nanoparticles, known as HPCNFs-N. The resulting material demonstrates exceptional electrochemical characteristics as an electrode material for supercapacitors, with remarkable specific capacitance across a range of current densities, high energy/power density, and long-term stability of over 10,000 cycles. These improvements are attributed to the unique structural features and superior chemical composition of the material [25].

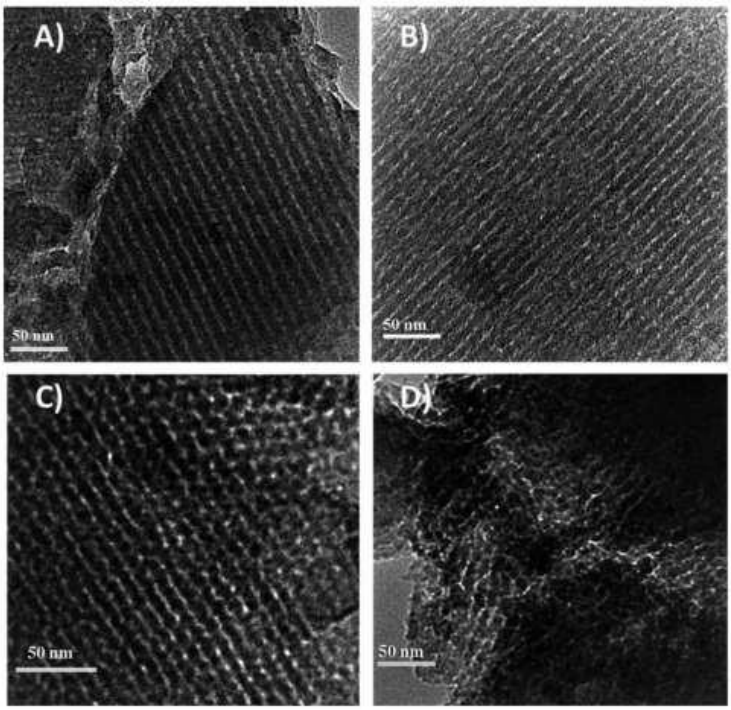

Figure 2.2. "TEM images of ": (a) NC0, (b) NC1, (c) NC2, and (d) NC3 showing Nitrogen Doped Carbon at Different Ratios [27]

A soft-templating hydrothermal method has been developed for synthesizing mesoporous carbon doped with nitrogen (N). This process employs D-Fructose and dicyandiamide (DCDA) as carbon and nitrogen precursors, respectively, and Pluronic F127 as the soft

template. Compared to undoped carbon material derived from the same process, the resulting N-doped mesoporous carbon exhibits significant improvement in electrical conductivity and specific capacitance, which reached 212 F g^{-1} at a scan rate of 1 mV s^{-1}. By adjusting the weight ratio of DCDA to D-Fructose, a tunable N-doping level (ranging from 4.5 to 14.5 wt%) and specific surface area (ranging from 375 to 730 m^2 g^{-1}) can be achieved. The study systematically investigates the factors impacting electrochemical performance, including specific surface area, electrical conductivity, and pseudocapacitance. The optimum N-doping level for achieving high electrochemical capacitance is found to be 6.0 wt% N-doping. This work provides insights into the effects of N-doping and interactions among the three factors affecting capacitance, which can guide the future design of electrode materials with improved electrochemical performance [27].

2.3.4 Graphene composites

The Graphene sheets are made up of hexagonal networks of carbon atoms, forming a two-dimensional structure. Graphene has numerous advantages over other materials. However, oxidation and adsorption shrink the surface area of the oxidized graphene sheets by stacking them back up. Further activation is necessary to increase the surface area by separating the graphene sheets from each other. High-temperature annealing can separate the sheets of graphene-oxide. In a recent study, GO/AC composites were synthesized in one step, resulting in an eight-fold increase in surface area after annealing. Graphene's electrochemical performance is also improved, compared to graphene without active carbon. By assembling graphene plates in a porous arrangement, mesopores can be created between microporous scaffolds, taking advantage of graphene's large surface area. This increased diffusion efficiency enhances the electrochemical performance. Electrodes made from this composite had three times higher energy density than those made from pristine activated carbon [28].

The Graphene's honeycomb-like lattice structure makes it an excellent template for creating 2D porous materials. Typically, Schiff-base chemistry is used to assemble porous organic materials. In a recent study, TPP was used as a precursor to fabricate supercapacitors with a capacitance of 430 F g^{-1} at a current density of 0.1 A g^{-1}[29].

The formation of a novel arrangement of hollow carbon atoms in a curved sheet-like assembly is worthy of discussion. The curved morphology of the particles prevents them from stacking together. Carbon capsules with this structure can be produced through nano-casting using silica atoms with a strong core and a matrix containing N-rich precursor, as shown in Figure 2.3. These carbon capsules exhibit excellent performance in an aqueous medium, with an efficiency of 240 F g^{-1} and a capacitance retention rate of 72% after 10,000cycles. At a current density of 100 A g^{-1}, these supercapacitors perform better in an organic medium, with a capacitance retention rate of 93% after 10,000 cycles [30]. Carbon-based materials have been extensively studied as supercapacitor electrodes. Graphene and CNTs have a vast surface area, which offers the potential for high specific EDL capacitance. However, using these materials alone presents certain engineering obstacles and yields only moderate volumetric capacitance in practical cells.

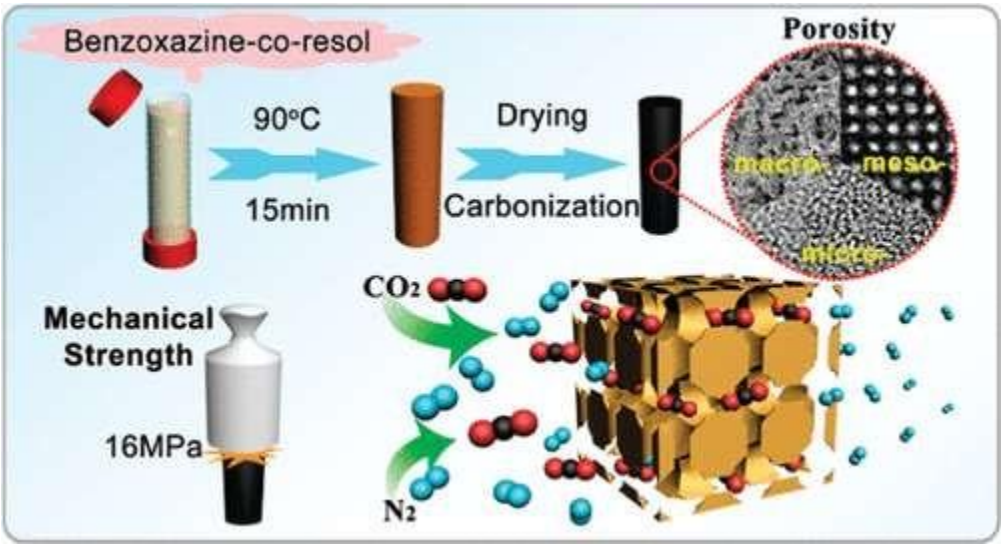

Figure 2.3. Synthesis of Carbon capsule [30].

The field has seen significant progress with the development of composite structures that combine different types of carbon. Such composite materials have the potential to not only produce practical electrodes but also to pave the way for the fabrication of porous structures with improved properties. In certain cases, the use of carbon-based composite electrodes resulted in nearly twice the capacitance compared to unmodified carbon electrodes. A prime example of this improvement is CNT-activated carbon composites. Mixing CNTs with electrode materials has been a long-standing practice.

Advancements in nanofabrication methods that enable the control of materials at an atomic scale and the ability to mass-produce nanomaterials are driving these approaches forward.

2.4 Metal-oxide composites

Metal oxides, such as Ru_2O_3, V_2O_5, Fe_3O_4, Co_3O_4, Ni_2O_3, and Ti_2O_2, have been extensively studied for their potential use in supercapacitors and hybrid devices. Unlike carbon materials that rely on the capacitive charge storage mechanism (EDL), metal oxides demonstrate pseudocapacitance. Activated carbon electrodes can be combined with oxides such as Co_3O_4, NiO, and TiO_2 to form battery-type electrodes. The redox behavior of these oxides is due to the multivalent nature of their transition metals, and they undergo reversible oxidation and reduction reactions with protons and/or hydroxide anions, which affects both the electrode surface and bulk of the oxides. However, metal oxides often have low conductivity and excellent specific capacitance or capacity. In contrast, carbon materials have relatively low specific capacitance but excellent conductivity. To overcome this limitation, nano metal oxides can be integrated with carbon structures to form a composite electrode with a conductive backbone that supports nanocomponents with high capacitance/capacity[31].

2.4.1 Cobalt oxide-based composites

This article examines the electrochemical properties and synthesis process of Co_3O_4/rGONS composites for supercapacitors. The Co_3O_4 nanosheets are fine nanoparticles that assemble uniformly and form a flower shape on the reduced graphene oxide surfaces. The electrochemical properties of the composites are analyzed using cyclic voltammetry and galvanostatic charge/discharge in a 1 M KOH aqueous solution. The Co_3O_4/rGONS composites exhibit superior specific capacity and redox performance compared to pure Co_3O_4, which is attributed to the high porosity of the composite structure due to the interaction between Co_3O_4 and reduced graphene oxide nanosheets during synthesis. The Co_3O_4/rGONS-II composite demonstrates good cyclic performance

with a better coulomb efficiency and a specific capacitance exceeding 400 F g^{-1} at a current density range of 0.5-2.0 A g^{-1}[34].

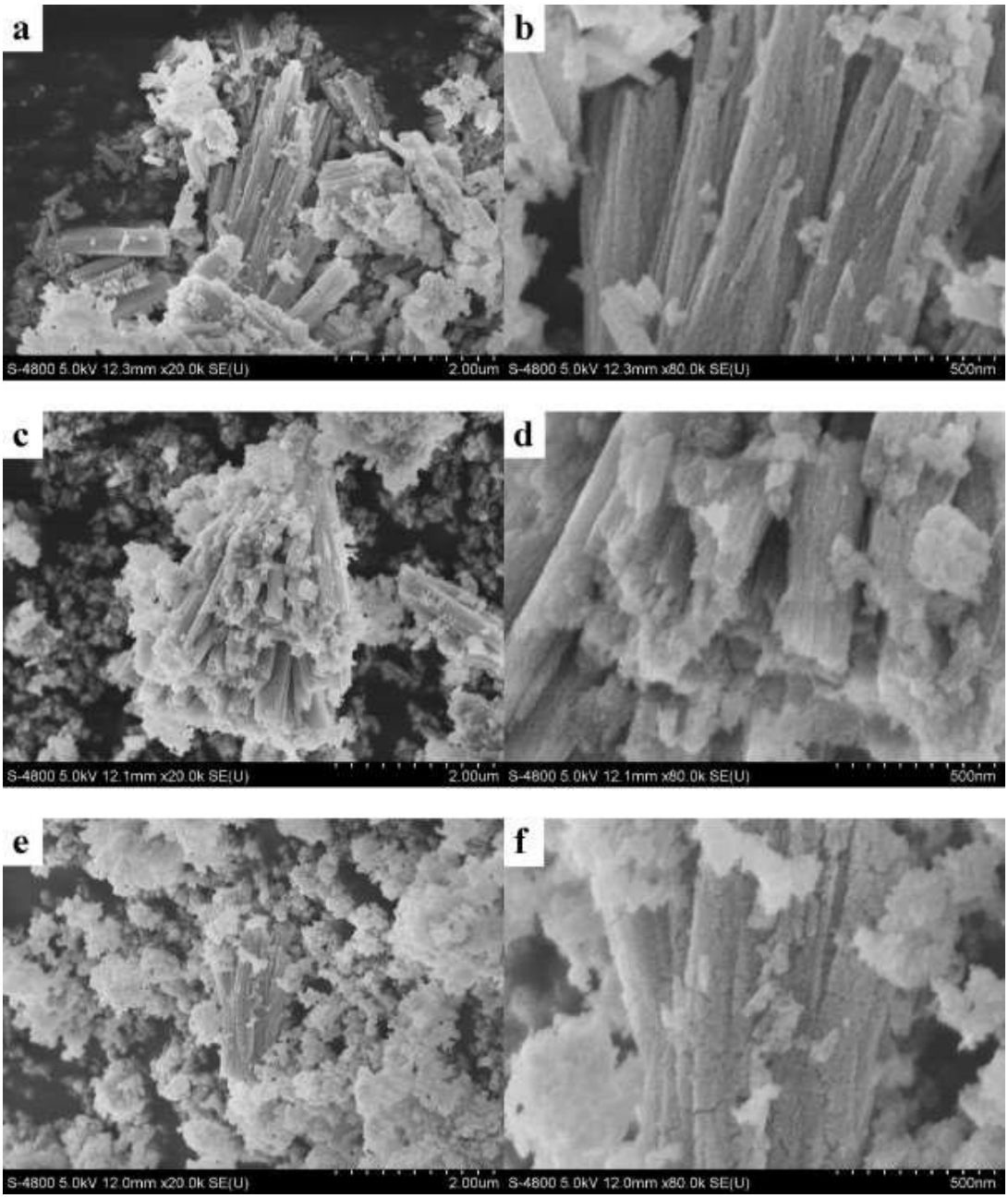

Figure 2.4. SEM images of Co_3O_4 (pure) (a, b), Co_3O_4/rGONS-II (c, d) and Co_3O_4/rGONS-IV (e, f) at different magnification [34].

This method has garnered considerable interest, such as the utilization of the solvothermal technique for producing an ultrafine Co_3O_4 nanoparticle material. These nanoparticles

exhibited a specific capacitance of 523.0 F g^{-1} at 0.5 A g^{-1}, along with excellent cycling stability, maintaining approximately 104.9% after 1500 cycles [35].

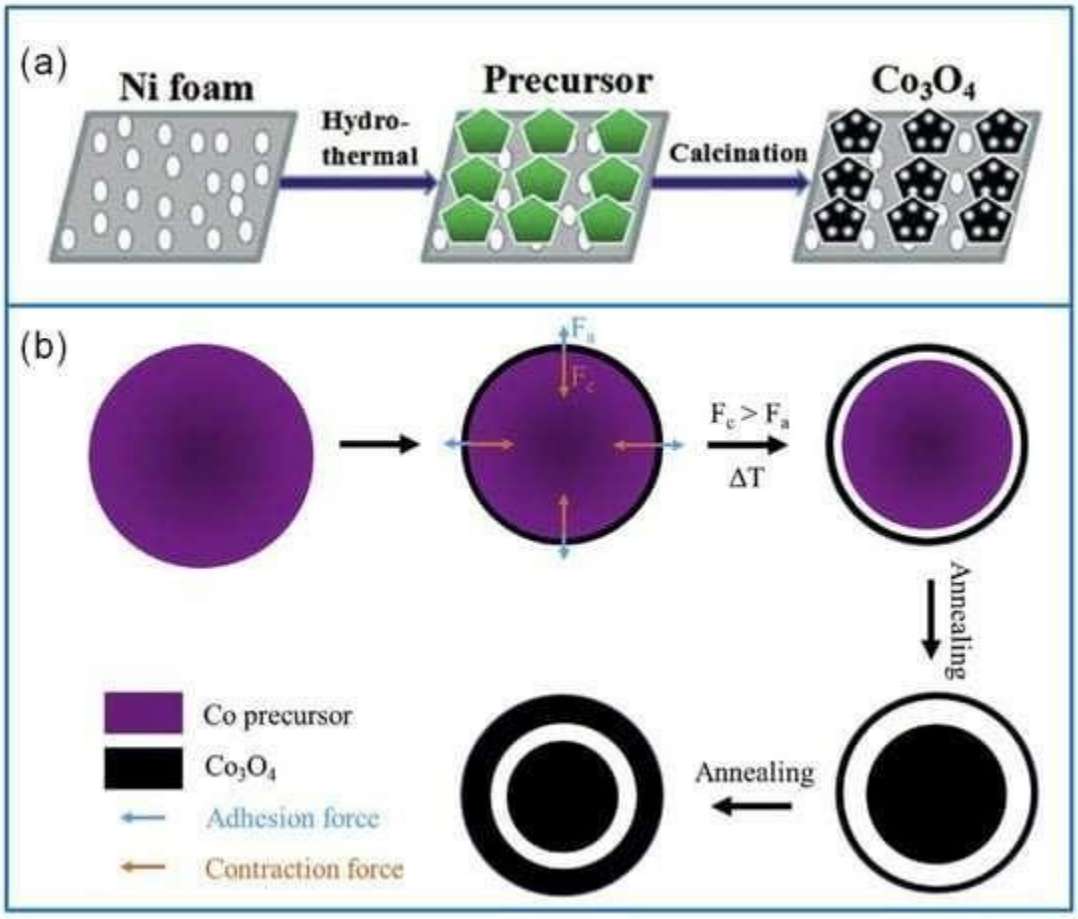

Figure 2.5. (a) Schematic diagram of preparing 2D ultrathin Co_3O_4 nanosheets using the hydrothermal method. (b) Schematic illustration of preparing core–shell Co_3O_4 mesoporous nanospheres using the solvothermal method [35]

2.4.2 Co-based composites

Experimental findings reveal that the energy storage performance of electrodes was considerably improved by the cooperative contributions of nanotubes, graphene, and cobalt substitution. The composite with a 50% Co and 50% Ni ratio (i.e., $Co_{0.5}Ni_{0.5}(OH)_2$) displayed a remarkable maximum specific capacitance of 2360 F g^{-1} (360 mA h g^{-1}) at 0.5 A g^{-1} and sustained a high specific capacitance of 2030 F g^{-1} at 20 A g^{-1} (~86% retention). The double hydroxides were able to modulate their redox behavior, which was influenced by the ratio between cobalt and nickel. These findings demonstrate the

significance of functional composites' rational design and large-scale assembly strategies in producing energy storage applications' enhanced performance and adjustability [36].

A two-step hydrothermal technique was utilized to prepare composite materials based on nickel-cobalt chalcogenides. The effect of adding 2D reduced graphene oxide (RGO) sheets and replacing the anion with selenium on the morphology and crystalline phase of the materials was investigated. The corresponding changes in physicochemical properties were also examined, and their relationship to the altered electrochemical properties was explored. The electrochemical properties of the materials were significantly improved when selenization was carried out in the presence of reduced graphene oxide (RGO) sheets. The $NiCo_2Se_4$/RGO (NCSG) electrode exhibited the highest specific capacitance of 1776 F g^{-1} at a current density of 2 A g^{-1} and maintained excellent specific capacitance (51%) even at high current densities of 50 A g^{-1}. When the NCSG was combined with sonochemically reduced graphene oxide (SRGO) to form a hybrid supercapacitor (HSC) (SRGO//NCSG), the device exhibited a high specific capacitance of magnitude 212 F g^{-1} at a current density of 2 A g^{-1} [37].

2.5 Metal–organic frameworks

The MOFs are multi-dimensional materials composed of metal centers connected by organic linkers. There may be several thousand square meters per gramme of surface area in some of these MOFs because of the development of void spaces within the coordination network of the organic molecules. They are, however, not widely used in electrochemical systems because of their non-conducting nature. We've already discussed the advantages of composite materials that combine both electrochemical and redox-active materials with conducting carbons. Fleker et al. synthesized MOF-activated carbon compositions to talk about nonconductive nature of MOFs, a result of the network's coordinating bonds. MOF nanoparticles in contact with activated carbon show an interesting EPR signal [22]. The MOF's Cu^{2+}/Cu^{+} redox couple increases the AC's double-layer capacitance by 30 percent. Yaghi et al. conducted a comprehensive study on the growth of MOF on graphene sets. Zirconium-MOF showed an aerial capacitance of 5.09 μF/cm for over 10,000 charge/discharge cycles [23].

Better composite materials may be produced by using wet or dry nanofabrication techniques. As organic nanoparticle fabrication techniques have become more

homogeneous and reproducible, they have transformed the pharmaceutical and medical industry. For complex composite materials, the rapid prototyping field opens up new possibilities. Of course, each technique must be adapted to fabricate high surface area electrodes, which requires additional development. The high surface area and porosity of MOFs provide numerous active sites for redox reactions, making them ideal for use in supercapacitor electrodes. Additionally, the structure and chemical composition of MOFs can be tailored to enhance their electrochemical properties, such as specific capacitance, energy density, and cycling stability. Overall, MOFs hold promise as a new class of electrode materials for supercapacitor devices, and ongoing research efforts are aimed at further optimizing their electrochemical performance for practical energy storage applications.

Summary

This chapter provides a brief summary of the characteristics of suitable electrode materials for supercapacitor devices, such as activated carbon, carbon nanotubes, polypyrrole (PPY), graphene, polyaniline (PANI), and polythiophene (PTH). Overall, the literature review chapter provided insights into the latest research on electrode materials for supercapacitors and highlighted the need for further research in this area to develop high-performance energy storage devices with longer lifetimes, higher energy densities, and better power densities.

List of References

1. P. Sinha and K. K. Kar, "Introduction to supercapacitors," in *Handbook of Nanocomposite Supercapacitor Materials II: Performance*: Springer, 2020, pp. 1-28.
2. A. K. Samantara and S. Ratha, "Materials development for Active/Passive components of a supercapacitor: background, present status and future perspective," 2017.
3. A. K. Samantara, S. Ratha, A. K. Samantara, and S. Ratha, "Historical background and present status of the supercapacitors," *Materials development for active/passive components of a supercapacitor: background, present status and future perspective*, pp. 9-10, 2018.
4. M. Wayu, "Manganese oxide carbon-based nanocomposite in energy storage applications," *Solids*, vol. 2, no. 2, pp. 232-248, 2021.
5. N. Lakal, S. Dubal, and P. Lokhande, "Supercapacitors: An introduction," *Nanotechnology in the Automotive Industry*, pp. 459-466, 2022.
6. P. Bhojane, "Recent advances and fundamentals of Pseudocapacitors: Materials, mechanism, and its understanding," *Journal of Energy Storage*, vol. 45, p. 103654,2022.
7. V. V. Jadhav, R. S. Mane, P. V. Shinde, V. V. Jadhav, R. S. Mane, and P. V. Shinde, "Electrochemical supercapacitors: history, types, designing processes, operation mechanisms, and advantages and disadvantages," *Bismuth-Ferrite-Based Electrochemical Supercapacitors*, pp. 11-36, 2020.
8. E. Piacenza, A. Presentato, and R. J. Turner, "Stability of biogenic metal (loid) nanomaterials related to the colloidal stabilization theory of chemical nanostructures," *Critical reviews in biotechnology*, vol. 38, no. 8, pp. 1137-1156, 2018.
9. M. Khot and A. Kiani, "A review on the advances in electrochemical capacitive charge storage in transition metal oxide electrodes for pseudocapacitors," *International Journal of Energy Research*, 2022.
10. L. Yin, S. Li, X. Liu, and T. Yan, "Ionic liquid electrolytes in electric double

layercapacitors," *Sci. China Mater,* vol. 62, no. 11, pp. 1537-1555, 2019.

11. S. Najib and E. Erdem, "Current progress achieved in novel materials for supercapacitor electrodes: mini review," *Nanoscale Advances,* vol. 1, no. 8, pp. 2817-2827, 2019.
12. S. Wu, J. Liu, H. Wang, and H. Yan, "A review of performance optimization of MOF-derived metal oxide as electrode materials for supercapacitors," *International Journal of Energy Research,* vol. 43, no. 2, pp. 697-716, 2019.
13. S. Zhang and N. Pan, "Supercapacitors performance evaluation," *Advanced Energy Materials,* vol. 5, no. 6, p. 1401401, 2015.
14. Q. Gou, S. Zhao, J. Wang, M. Li, and J. Xue, "Recent advances on boosting the cell voltage of aqueous supercapacitors," *Nano-Micro Letters,* vol. 12, pp. 1-22, 2020
15. A. Jänes, H. Kurig, and E. Lust, "Characterisation of activated nanoporous carbon for supercapacitor electrode materials," *Carbon,* vol. 45, no. 6, pp. 1226-1233, 2007.
16. C. Zhu *et al.*, "All metal nitrides solid-state asymmetric supercapacitors," *Advanced Materials,* vol. 27, no. 31, pp. 4566-4571, 2015.
17. K. D. Verma, P. Sinha, S. Banerjee, and K. K. Kar, "Characteristics of electrode materials for supercapacitors," in *Handbook of Nanocomposite Supercapacitor Materials I: Characteristics*: Springer, 2020, pp. 269-285.
18. Y. Zhang *et al.*, "Progress of electrochemical capacitor electrode materials: A review," *International journal of hydrogen energy,* vol. 34, no. 11, pp. 4889-4899, 2009.
19. E. Sharmin and F. Zafar, "Introductory chapter: metal organic frameworks (MOFs)," in *Metal-organic frameworks*: IntechOpen, 2016.
20. M. S. Kolathodi and T. S. Natarajan, "Development of high-performance flexible solid state supercapacitor based on activated carbon and electrospun TiO2 nanofibers," *Scripta Materialia,* vol. 101, pp. 84-86, 2015.
21. Y. Wang, Z. Chang, M. Qian, Z. Zhang, J. Lin, and F. Huang, "Enhanced specific capacitance by a new dual redox-active electrolyte in activated carbon-based supercapacitors," *Carbon,* vol. 143, pp. 300-308, 2019.

22. J. Ben, Z. Song, X. Liu, W. Lü, and X. Li, "Fabrication and electrochemical performance of PVA/CNT/PANI flexible films as electrodes for supercapacitors," *Nanoscale Research Letters,* vol. 15, pp. 1-8, 2020.
23. H. Li *et al.*, "Enhanced electrochemical performance of CuCo2S4/carbon nanotubes composite as electrode material for supercapacitors," *Journal of colloid and interface science,* vol. 549, pp. 105-113, 2019.
24. P. Wu *et al.*, "A low-cost, self-standing NiCo2O4@ CNT/CNT multilayer electrode for flexible asymmetric solid-state supercapacitors," *Advanced Functional Materials,* vol. 27, no. 34, p. 1702160, 2017.
25. R. Ahmad, N. Iqbal, M. M. Baig, T. Noor, G. Ali, and I. H. Gul, "ZIF-67 derived nitrogen doped CNTs decorated with sulfur and Ni (OH) 2 as potential electrode material for high-performance supercapacitors," *Electrochimica Acta,* vol. 364, p. 137147, 2020.
26. Y. Hu, H. Liu, Q. Ke, and J. Wang, "Effects of nitrogen doping on supercapacitor performance of a mesoporous carbon electrode produced by a hydrothermal soft-templating process," *Journal of Materials Chemistry A,* vol. 2, no. 30, pp. 11753-11758, 2014.
27. A. Ramadoss and S. J. Kim, "Improved activity of a graphene–TiO2 hybrid electrode in an electrochemical supercapacitor," *Carbon,* vol. 63, pp. 434-445, 2013.
28. A. Borenstein, O. Hanna, R. Attias, S. Luski, T. Brousse, and D. Aurbach, "Carbon-based composite materials for supercapacitor electrodes: a review," *Journal of Materials Chemistry A,* vol. 5, no. 25, pp. 12653-12672, 2017.
29. G.-P. Hao *et al.*, "Structurally designed synthesis of mechanically stable poly (benzoxazine-co-resol)-based porous carbon monoliths and their application as high-performance
30. CO2 capture sorbents," *Journal of the American Chemical Society,* vol. 133, no. X. Lu et al., "Hydrogenated TiO2 nanotube arrays for supercapacitors," Nano letters, vol. 12, no. 3, pp. 1690-1696, 2012.
31. C. C. Raj and R. Prasanth, "advent of TiO2 nanotubes as supercapacitor electrode,"Journal of The Electrochemical Society, vol. 165, no. 9, p. E345, 2018.

32. Z. Song et al., "Hydrothermal synthesis and electrochemical performance of Co3O4/reduced graphene oxide nanosheet composites for supercapacitors," Electrochimica Acta, vol. 112, pp. 120-126, 2013.
33. X. Wang, A. Hu, C. Meng, C. Wu, S. Yang, and X. Hong, "Recent advance in Co3O4 and Co3O4-containing electrode materials for high-performance supercapacitors," Molecules, vol. 25, no. 2, p. 269, 2020.

34. X. Lu *et al.*, "Hydrogenated TiO2 nanotube arrays for supercapacitors," *Nano letters*, vol. 12, no. 3, pp. 1690-1696, 2012.
35. C. C. Raj and R. Prasanth, "advent of TiO2 nanotubes as supercapacitor electrode," *Journal of The Electrochemical Society*, vol. 165, no. 9, p. E345, 2018.
36. Z. Song *et al.*, "Hydrothermal synthesis and electrochemical performance of Co3O4/reduced graphene oxide nanosheet composites for supercapacitors," *Electrochimica Acta*, vol. 112, pp. 120-126, 2013.
37. X. Wang, A. Hu, C. Meng, C. Wu, S. Yang, and X. Hong, "Recent advance in Co3O4 and Co3O4-containing electrode materials for high-performance supercapacitors," *Molecules*, vol. 25, no. 2, p. 269, 2020.
38. Y. Cheng, H. Zhang, C. V. Varanasi, and J. Liu, "Improving the performance of cobalt–nickel hydroxide-based self-supporting electrodes for supercapacitors using accumulative approaches," *Energy & Environmental Science*, vol. 6, no. 11, pp. 3314-3321, 2013.
39. S. Ghosh, P. Samanta, N. C. Murmu, and T. Kuila, "Investigation of electrochemical charge storage in nickel-cobalt-selenide/reduced graphene oxide composite electrode and its hybrid supercapacitor device," *Journal of Alloys and Compounds*, vol. 835, p. 155432, 2020.
40. Z. Li, L. Y. Zhang, L. Zhang, J. Huang, and H. Liu, "ZIF-67-derived CoSe/NC composites as anode materials for lithium-ion batteries," *Nanoscale Research Letters*, vol. 14, pp. 1-11, 2019.
41. Q. Yang, R. Lu, S. Ren, C. Chen, Z. Chen, and X. Yang, "Three dimensional reduced graphene oxide/ZIF-67 aerogel: Effective removal cationic and anionic dyes from water," *Chemical Engineering Journal*, vol. 348, pp. 202-211, 2018.
42. Y. Zhang *et al.*, "Nitrogen-doped yolk–shell-structured CoSe/C dodecahedra for high-performance sodium ion batteries," *ACS applied materials & interfaces*, vol. 9, no. 4, pp. 3624-3633, 2017.
43. Y. Miao *et al.*, "Polyhedral NiCoSe2 synthesized via selenization of metal-organic framework for supercapacitors," *Materials Letters*, vol. 242, pp. 42-46, 2019.
44. Q. Wang *et al.*, "ZIF-67 derived amorphous CoNi2S4 nanocages with nanosheet arrays on the shell for a high-performance asymmetric supercapacitor," *Chemical Engineering Journal*, vol. 327, pp. 387-396, 2017.

45. R. Ahmad *et al.*, "Zeolitic imidazolate frameworks derived Co-Zn-nanoporous carbon-sulfide material for supercapacitors," *Electrochimica Acta,* vol. 404, p. 139739, 2022.
46. F. Zheng, Y. Yang, and Q. Chen, "High lithium anodic performance of highly nitrogen-doped porous carbon prepared from a metal-organic framework," *Nature communications,* vol. 5, no. 1, p. 5261, 2014.
47. X. Wang *et al.*, "MOF derived catalysts for electrochemical oxygen reduction," *Journal of Materials Chemistry A,* vol. 2, no. 34, pp. 14064-14070, 2014.
48. A. A. Ensafi, N. Ahmadi, and B. Rezaei, "Electrochemical preparation and characterization of a polypyrrole/nickel-cobalt hexacyanoferrate nanocomposite for supercapacitor applications," *RSC advances,* vol. 5, no. 111, pp. 91448-91456, 2015.
49. J. Wang, J. Polleux, J. Lim, and B. Dunn, "Pseudocapacitive contributions to electrochemical energy storage in TiO2 (anatase) nanoparticles," The Journal of Physical Chemistry C, vol. 111, no. 40, pp. 14925-14931, 2007.
50. J. Yang and S. Gunasekaran, "Electrochemically reduced graphene oxide sheets for use in high performance supercapacitors," Carbon, vol. 51, pp. 36-44, 2013.
51. R. Wang et al., "Electrochemical properties of manganese ferrite-based supercapacitors in aqueous electrolyte: the effect of ionic radius," Colloids and Surfaces A: Physicochemical and Engineering Aspects, vol. 457, pp. 94-99, 2014.
52. M. Itagaki, S. Suzuki, I. Shitanda, and K. Watanabe, "Electrochemical impedance and complex capacitance to interpret electrochemical capacitor," Electrochemistry, vol. 75, no. 8, pp. 649-655, 2007.
53. J. Wang, J. Polleux, J. Lim, and B. Dunn, "Pseudocapacitive contributions to electrochemical energy storage in TiO2 (anatase) nanoparticles," The Journal of Physical Chemistry C, vol. 111, no. 40, pp. 14925-14931, 2007.
54. J. Yang and S. Gunasekaran, "Electrochemically reduced graphene oxide sheets for use in high performance supercapacitors," Carbon, vol. 51, pp. 36-44, 2013.
55. R. Wang et al., "Electrochemical properties of manganese ferrite-based supercapacitors in aqueous electrolyte: the effect of ionic radius," Colloids and Surfaces A: Physicochemical and Engineering Aspects, vol. 457, pp. 94-99, 2014

56. J. Wang, J. Polleux, J. Lim, and B. Dunn, "Pseudocapacitive contributions to electrochemical energy storage in TiO2 (anatase) nanoparticles," *The Journal of Physical Chemistry C,* vol. 111, no. 40, pp. 14925-14931, 2007.
57. J. Yang and S. Gunasekaran, "Electrochemically reduced graphene oxide sheets for use in high performance supercapacitors," *Carbon,* vol. 51, pp. 36-44, 2013.
58. R. Wang *et al.,* "Electrochemical properties of manganese ferrite-based supercapacitors in aqueous electrolyte: the effect of ionic radius," *Colloids and Surfaces A: Physicochemical and Engineering Aspects,* vol. 457, pp. 94-99, 2014.
59. M. Itagaki, S. Suzuki, I. Shitanda, and K. Watanabe, "Electrochemical impedance and complex capacitance to interpret electrochemical capacitor," *Electrochemistry,* vol. 75, no. 8, pp. 649-655, 2007.
60. Y. Zhang *et al.,* "Self-templated synthesis of N-doped CoSe2/C double-shelled dodecahedra for high-performance supercapacitors," *Energy Storage Materials,* vol. 8, pp. 28-34, 2017.
61. Z. Qu, J. Li, M. Guo, L. Zhao, L. Duan, and S. Ding, "Design tremella-like Ni-Co selenide with wonderful electrochemical performances as supercapacitor cathode material," *Electrochimica Acta,* vol. 393, p. 139049, 2021.
62. X. Zhang, J. Gong, K. Zhang, W. Zhu, J.-C. Li, and Q. Ding, "All-solid-state asymmetric supercapacitor based on porous cobalt selenide thin films," *Journal of Alloys and Compounds,* vol. 772, pp. 25-32, 2019.
63. S. Wu *et al.,* "One-pot synthesis of the flower-like Co0. 85Se nanosheets as an anode material for long-life aqueous asymmetric supercapacitor," *Synthetic Metals,* vol. 268, p. 116499, 2020.
64. H. Chen, W. Li, M. He, X. Chang, X. Zheng, and Z. Ren, "Vertically oriented carbon nanotube as a stable frame to support the Co0. 85Se nanoparticles for high performance supercapacitor electrode," *Journal of Alloys and Compounds,* vol. 855, p. 157506, 2021.

Chapter 3: Review on Experimentation and Characterization Methods

3.1 Synthesis Method

For the proper synthesis of the catalyst material in the lab, many methods have been devised. Among them, some methods require special equipment while others can be performed without them. Choice of the catalyst synthesis process to form required NPs mainly rests on the preferred size, suitable properties of the surface, and the kind of material that is concerned such as semiconductors, metals, polymers, ceramics, etc. These methods have been researched and improved to increase the yield of our catalyst, obtain better structural properties and purity. Some of these methods have been discussed below:

3.1.1 Solvothermal Synthesis

It is a technique used for making a range of materials like semiconductors, metals, polymers, and ceramics. The method involves a solvent at moderate to high pressure (typically between 1atm and 10,000 atm) and temperature (from 100 °C to 1000 °C) whichhelps precursors in interaction during synthesis. If the solvent used is water, then the process is known as the "hydrothermal process." The conditions of the hydrothermal synthesis process are usually kept at the supercritical temperature of water (374 °C). This method can be performed to make a wide variety of geometries such as thin films, single crystals, bulk powders, and nanocrystals. In addition, the formation (rod (2D), sphere (3D), and wire (1D) of crystals are organized by the control of chemical of interest concentration, solvent supersaturation, and control on kinetic. It can be used to form stagnant and thermodynamically stable forms involving novel elements that are not easily constructed from other synthetic paths. This review will emphasize some recent advances including the solvothermal process and nanocrystalline because in the last decade 80% of the literature focused on nanocrystals [1].

3.1.1.1 Synthesis of ZIF-67

ZIF-67 is usually prepared using solvothermal method. Simple scheme is used to synthesize ZIF-8. Metal salt cobalt nitrate hexahydrate is mixed with methanol to form a

solution. Organic linker 2-methyleimidazole is separately mixed with methanol to form another solution. Ratio of metal salt and organic linker is varied according to the morphology requirement and application. After that both solutions are mixed at room temperature while stirring. After 30 minutes of stirring solution is placed for 24 hours aging. After aging is finished purple precipitate settles down. Precipitate is thoroughly washed with ethanol and deionized water. Collected precipitate is dried in vacuum oven at 60 ℃ for 12 hours. After vacuum drying, sample is grinded to collect fine powder.

3.1.2 Hydrothermal Synthesis

This method is used to synthesize materials that require special conditions for the synthesis. Also, this method helps control the structure, morphology, and other properties of the material. Metal oxides, halides, composites that require specific temperature as well as pressure are usually synthesized by this method. The nanoparticles obtained by this method have characteristic properties. This method normally requires the use of an autoclave device in which temperature and pressure can be simultaneously controlled. The main significance of this process is the ability to synthesize a wide number of NPs that have upgraded composition, size, structure, and chemistry of surface that is reasonably cheap.

3.1.3 Pyrolysis

During pyrolysis, organic matter is decomposed into no condensable gases, condensable liquids, and biochar or charcoal as a residual solid product in an inert environment without oxygen.

3.1.4 Carbonization

Carbonization is a thermal decomposition process that produces a carbonaceous residue (while simultaneously removing the distillate) from organic substances. Pyrolysis is the oldest direct method of producing liquids from coal. It involves heating coal and capturing volatilized liquids, leaving behind a hydrogen-depleted carbon residue. In addition to the small amount of liquid that is produced (less than 20 percent), the mixture of chemicals and water contamination makes for a poor product. While organic matter is decomposed at high temperatures and the distillate is removed at the same time, carbonization is

primarily used to produce a carbonaceous residue known as coke. Carbonization of ZIF is performed to covert ZIF in to nano porous carbon and carbon nano tubes.

3.2 Characterization Techniques

3.2.1 X-Ray Diffraction (XRD)

This is one of the most important and common material characterization technique which provides information about the morphology, components, and crystallite size of the material. It uses X-ray radiations that pass through the material at an angle to the source. The diffraction angle is calculated, and the intensity is recorded. At an angle how many radiations deflect from a specific plane on the material gives information regarding its structure morphology.

To find evidence about the configuration of X-ray diffraction (XRD) of crystalline materials depend on the double particle/wave nature of X-rays. Identification and characterization of materials centered on their X-ray form are the major uses of the procedure. When a monochromatic X-rays incident beam contacts an object material the first outcome that takes place is atoms within the target substance scatter those X-rays as shown in Figure 3.1. The spread X-rays undertake destructive and constructive interference in the substances having proper structure (i.e. crystalline), which is called diffraction. The X-rays diffraction by crystals is described by Bragg‟s Law,

$$n(\lambda) = 2d\ Sin(\theta) \qquad (2)$$

The shape and size of the materials unit cell determine directions of likely diffractions. The atom's arrangement in the crystal structure affects the diffracted wave intensities. Many materials are not one crystal rather are comprised of little, small crystallites in all likely directions which are called polycrystalline powder or aggregate. When a material with casually focused crystallites is put in an X-ray, the beam will view all available interatomic planes. If the experimental angle is scientifically altered, then all the available diffraction peaks from the substance will be identified [2].

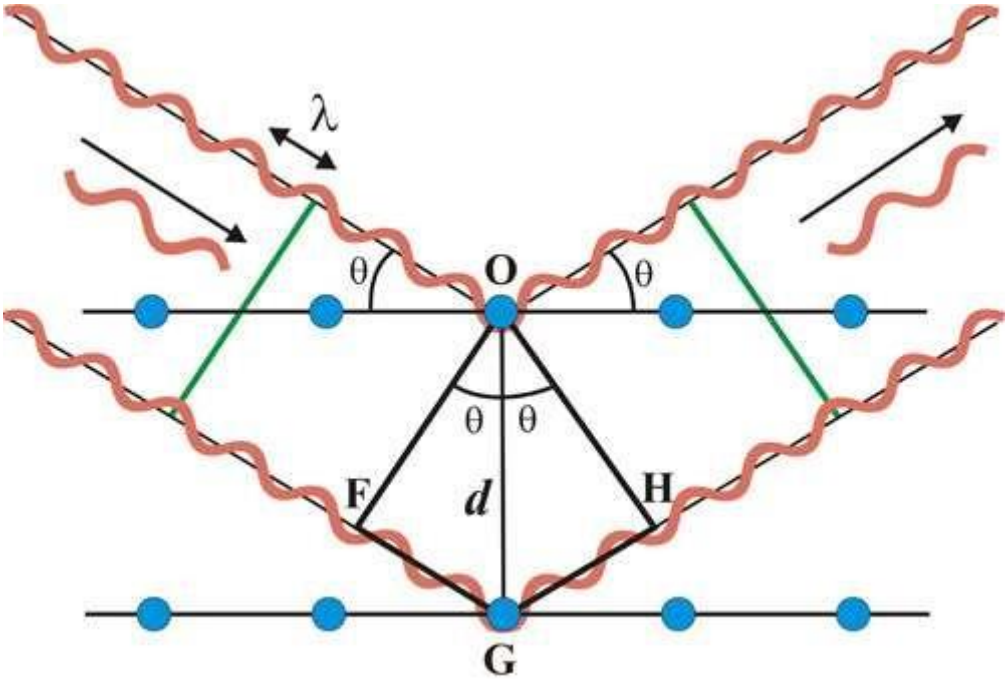

Figure 3.1. The Bragg's Law [1]

3.2.2 Scanning Electron Microscopy

The scanning electron microscope (SEM) uses a high-energy electrons-focused ray to produce a wide range of signals at the solid surface of the specimen. The high-energy electrons penetrate through the material and escape through the other end as shown in Figure 3.2. The information of the substance like chemical composition, crystalline structure, external morphology (texture), and materials orientation will be revealed signals of the electron beam and sample interactions. In various applications, a 2-dimensional image is formed that shows spatial variations in the properties, and numbers are collected over a particular choice area of the sample surface. The scanning method by simple SEM practices (magnification varying from 20X to around 30,000X, 3-D resolution of 50 to 100 nm) can be used to distinguish the areas that vary in size from about 1 cm to 5 microns in breadth. This method is exclusively valuable in semi quantitatively or qualitatively identifying chemical contents (by EDS), crystal orientations (using EBSD), and crystalline structure. The SEM is proficient in executing analyses of a specific area or point locations on the sample object. Its design and function are quite comparable to the EPMA and significant connections in abilities remain between the two devices [3].

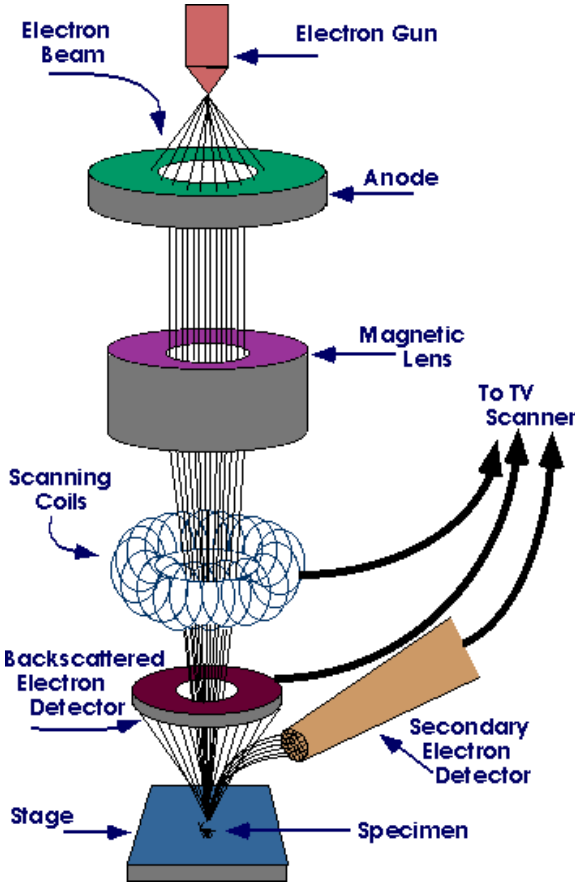

Figure 3.2. Illustration of how SEM works [2].

3.2.3 Energy Dispersive X-ray Spectroscopy (EDX)

EDS is an elemental analysis method used to quantify the number of individual elements present in a nanoparticle. This technique gives the number of substances at a particular point but does not give the overall quantity of each element. It is usually combined with SEM or TEM to get a nanoscale image of particles through them, and EDS performs the analysis of that nanostructure. In the early 1970s, EDS developed into one commercial product and rapidly crossed WDS in popularity. The overall structure of the EDS is very simple because of no moving parts like the rotation detector in WDS. The sensor gathers the X-rays energies signal from all series elements in a sample at a similar time as compared to gathering signals from X-ray wavelength one by one which makes the EDS systems relatively fast as seen in Figure 3.3. The characteristic energy dispersion resolution is around 150–200 eV, which is lower than WDS resolve. The lightest

component that can be identified is not C (Z=6) rather O (Z=8). But major benefits like low cost and fast analysis make these disadvantages insignificant [2].

EDS band is a graph between the power of X-rays and the corresponding energies. Both light and heavy elements can be seen in a range of spectrum from 0.1 to 10-20 keV because both M or L lines of heavy elements and K lines of light elements are evident in this array.

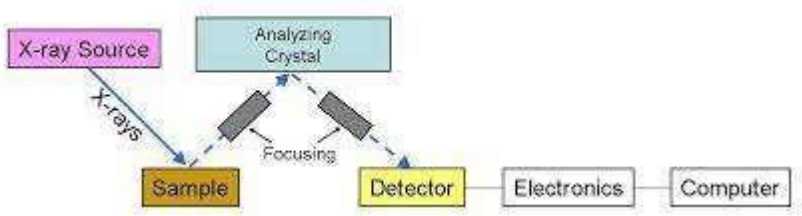

Figure 3.3. Illustration of EDX [3].

3.2.4 Thermo-Gravimetric Analysis

Thermogravimetric analysis (TGA) determines weight losses in a material with a change in temperature in a controlled atmosphere. The major applications of this characterization technique are the measurement of thermal stability, volatile content, moisture, organic linker in a sample, and the percent composition of components in a compound. The principle is that the temperature is gradually increased from zero to the required final temperature in a specific gas atmosphere which maybe Ar, air or some other gas. Now when temperature increases the contents in the sample start to evaporate. Moisture is usually the first content that removes from the sample so a change in mass of sample occurs. This mass is measured on the weight balance continuously during the process which is placed outside the furnace Figure 3.4. After moisture other volatile contents like organic residues start to escape. The stability of the sample can be defined as the temperature at which the material starts to decompose which is the main point in the curve. After that the line drops sharply causing a major loss in material. This point is called the decomposition temperature and determines the stability of material. The weight of the material is mapped against temperature or time to demonstrate the thermal changes in the sample, for instance, the loss of solvent, loss of water of hydration, and the decomposition of the material. At the end of the process, the final mass residue is noted, and the total mass loss is calculated [4].

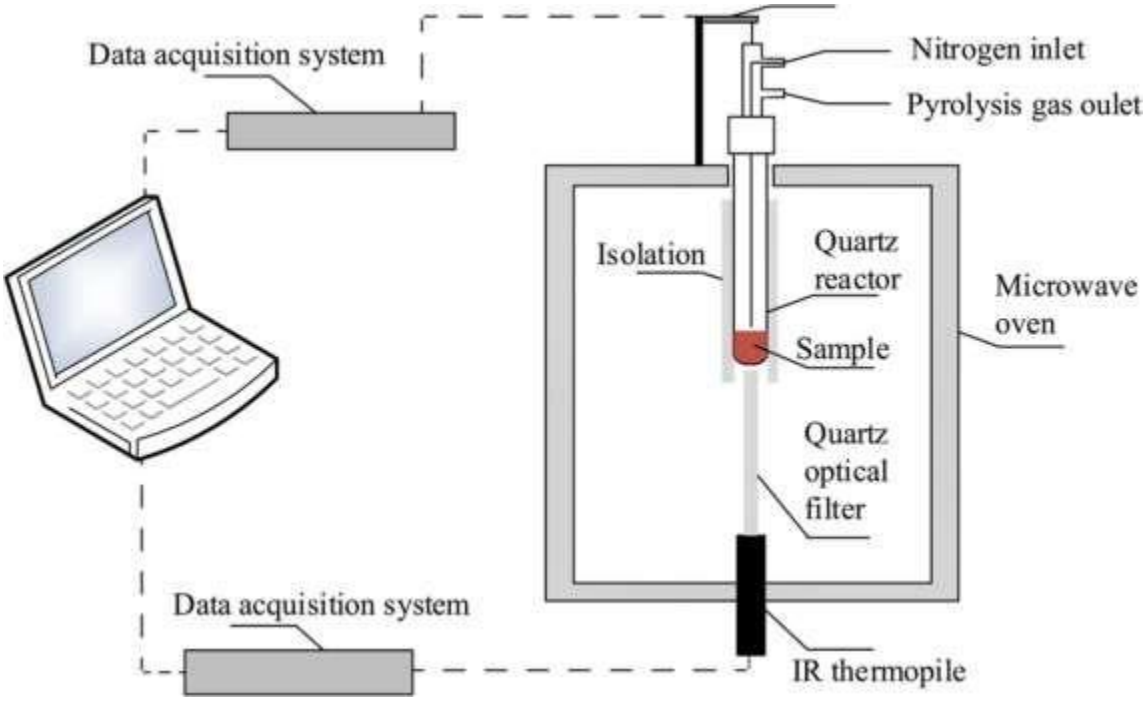

Figure 3.4. Schematic of TGA [4].

3.2.5 X-ray Photoelectron Spectroscopy

X-ray photoelectron spectroscopy (XPS) is a surface analysis technique used to determine the chemical composition of a material. XPS works by irradiating a sample surface with a beam of X-rays, which causes the ejection of electrons from the surface atoms. The ejected electrons, called photoelectrons, are then collected and analyzed based on their kinetic energy and the angles at which they are detected. In XPS, the energy of the X-ray beam is typically set to a value greater than the binding energy of the electrons in the sample's outermost energy level, or valence band. When an X-ray photon with sufficient energy is absorbed by an atom, it can cause an electron from the valence band to be ejected, leaving behind a positively charged ion. The ejected photoelectron will carry information about the electronic structure of the atom it came from, including the chemical composition and bonding environment.

The kinetic energy of the ejected photoelectrons is measured using an electron analyzer, which separates the photoelectrons based on their kinetic energy and direction of emission. The energy of the photoelectron is related to the binding energy of the electron in the original atom, and this information can be used to determine the chemical state and composition of the atoms in the sample surface. XPS can be used to identify the elements

present in a sample, as well as the oxidation state and chemical environment of those elements. It is a highly sensitive technique, capable of detecting even trace amounts of impurities or surface contaminants. XPS is widely used in materials science, surface chemistry, and semiconductor research to characterize the surfaces of materials, including metals, semiconductors, and polymers.

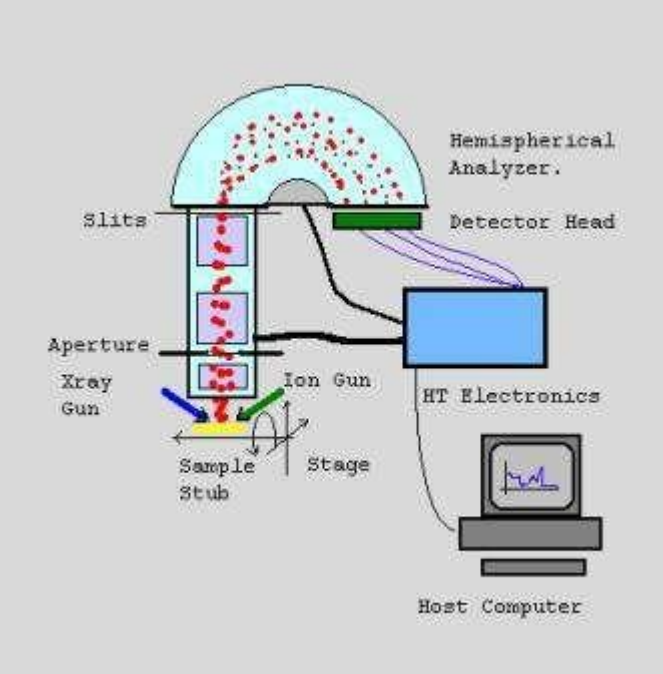

Figure 3.5. Schematic of XPS [4]

3.2.6 Transmission Electron Microscopy (TEM)

TEM (transmission electron microscopy) is an imaging technique that allows for high-resolution imaging of materials at the nanoscale. The technique involves passing a beam of electrons through a thin sample, which interacts with the electrons and creates an image based on the interaction. In a TEM, a beam of high-energy electrons is generated by an electron gun and focused by a series of electromagnetic lenses onto a thin sample. As the electrons pass through the sample, some are scattered, absorbed, or transmitted based on the density and thickness of the material. The transmitted electrons are then focused by additional lenses onto a fluorescent screen or a digital camera, producing a highly magnified image of the sample. TEM allows for the visualization of the internal structure of materials at atomic-scale resolution, as well as the observation of defects, dislocations, and other structural features that are difficult to observe with other techniques. It can also

be used to determine the crystal structure and orientation of materials, and to analyze the composition of materials using energy-dispersive X-ray spectroscopy (EDS) [3].

3.3 Electrochemical Testing

3.4 Electrochemical Testing for supercapacitors

3.4.1 Three-Electrode System

The three-electrode system is a widely used method for testing the performance of supercapacitors. This system comprises three electrodes: a working electrode, a reference electrode, and a counter electrode. The working electrode is the one being tested and is typically made of a high surface area material like activated carbon. A noble metal like platinum is commonly used for the reference electrode, which monitors the potential of the working electrode. On the other hand, the counter electrode is usually made of a conductive material such as a metal foil and is responsible for balancing the charges on the working electrode. The three-electrode system is particularly suitable for testing supercapacitor electrodes because it enables precise measurement of electrochemical behavior and capacitance. The reference electrode ensures accurate control of the potential on the working electrode, and the counter electrode guarantees that the charges are balanced for reliable capacitance measurement. It's important to note that in a three-electrode cell, the applied potential on the working electrode is given according to the reference electrode used and is entirely applied to the working electrode [15].

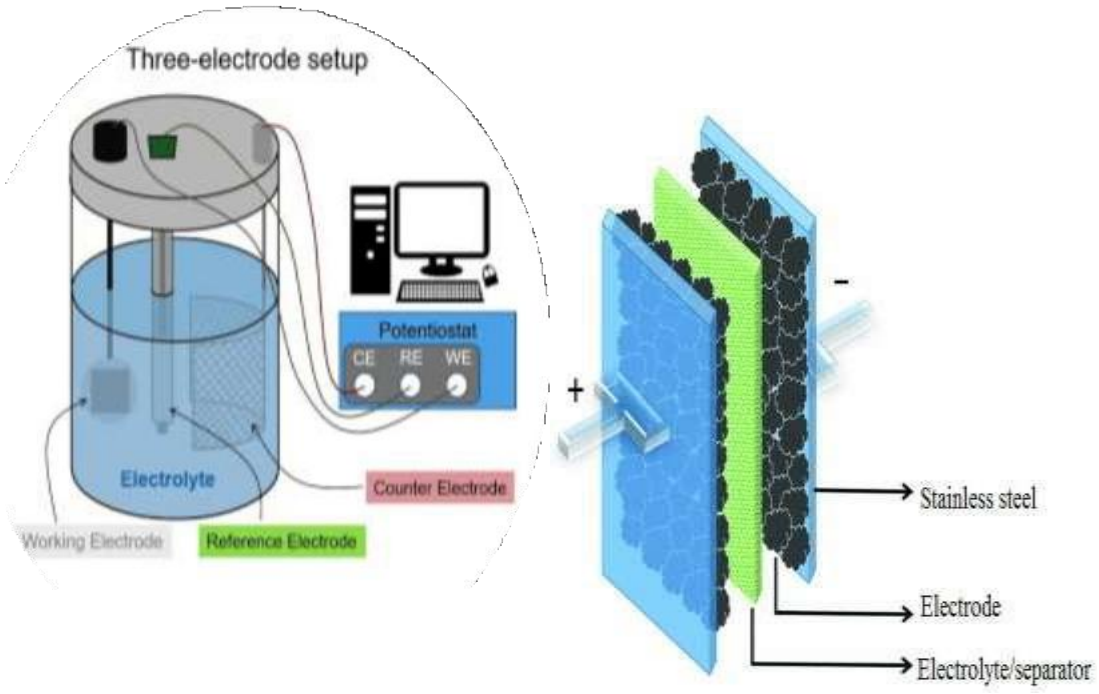

Figure 1.6. A three-electrode Beaker cell (left) and Two-Electrode System (Right) [16].

3.4.2 Two-Electrode System

When assessing the electrochemical activity of a packaged supercapacitor cell, using a two-electrode test fixture allows for a more accurate evaluation of its performance. Two-electrode test fixtures can either be commercially purchased or made using two stainless steel plates. In contrast, a three-electrode cell only permits the analysis of the working electrode, while a two-electrode configuration enables separate analysis of both electrodes. The electric potential applied to the system is equally distributed across every electrode in a two-electrode cell. On the other hand, in a three-electrode cell, the working electrode is subjected to twice the potential range of a two-electrode cell, resulting in a doubled capacitance calculation. Furthermore, in a two-electrode cell, when the reference electrode (RE) and working electrode (WE) are in close proximity, the RE can precisely control the interfacial potential. These parameters are employed to assess supercapacitor performance at the packaged cell level. [17].

3.4.3 Slurry/Ink Formation

There are many substrates available for using as working electrode for example Glassy carbon electrode, nickel foam and carbon cloth. For every substrate method of ink formation is different. For glassy carbon we use ethanol as solvent and nafion (5 wt.% ion solution in lower aliphatic alcohols) as binder. Purpose of binder is to bind the active electrode material so that it sticks to the electrode. For nickel foam and carbon cloth we use PVDF as binder and n-methylepropyrilidine (NMP) as solvent. Carbon black/graphite powder/super-p is also added to the slurry. PVDF binder causes resistance that ultimately mitigate the overall conductivity of the active material. Purpose of carbon black is to cope with the reduced activity of active material caused by the PVDF binder. After mixing the required recipe, solution is sonicated for 4 hours to make homogenous suspension.

3.5 Electrochemical Techniques

When glassy carbon electrode is fabricated, it is dried at 60 degrees Celsius for 30 minutes. After that electrochemical testing is performed. For super capacitors three techniques are performed in electrochemical workstation.

- Cyclic Voltammetry (CV)
- Chronopotentiometry
- Electrochemical Impedance Spectroscopy (EIS)

3.5.1 Cyclic Voltammetry

Cyclic voltammetry (CV) is a great and common technique of electrochemistry usually used to study the oxidation and reduction procedures of molecular species. It is helpful to investigate chemical reactions initiated by electron transfer, which comprises catalysis. This electrochemical technique involves the running of the workstation through a complete cycle. The potential range was input into the software which is applied across the two electrodes. Scan rate, sample interval, sensitivity was given for each run along with several segments. Two segments make one complete cycle. The cyclic voltammetry gives information of the current changing with voltage as shown in Figure 3.6 [10]. When CV is performed the current passes through an external circuit and electrons start to flow

from anode to cathode. For CV, beaker cell was used in three electrode system. Working electrode was glassy carbon, counter electrode was platinum wire and reference electrode was Ag/AgCl [6].

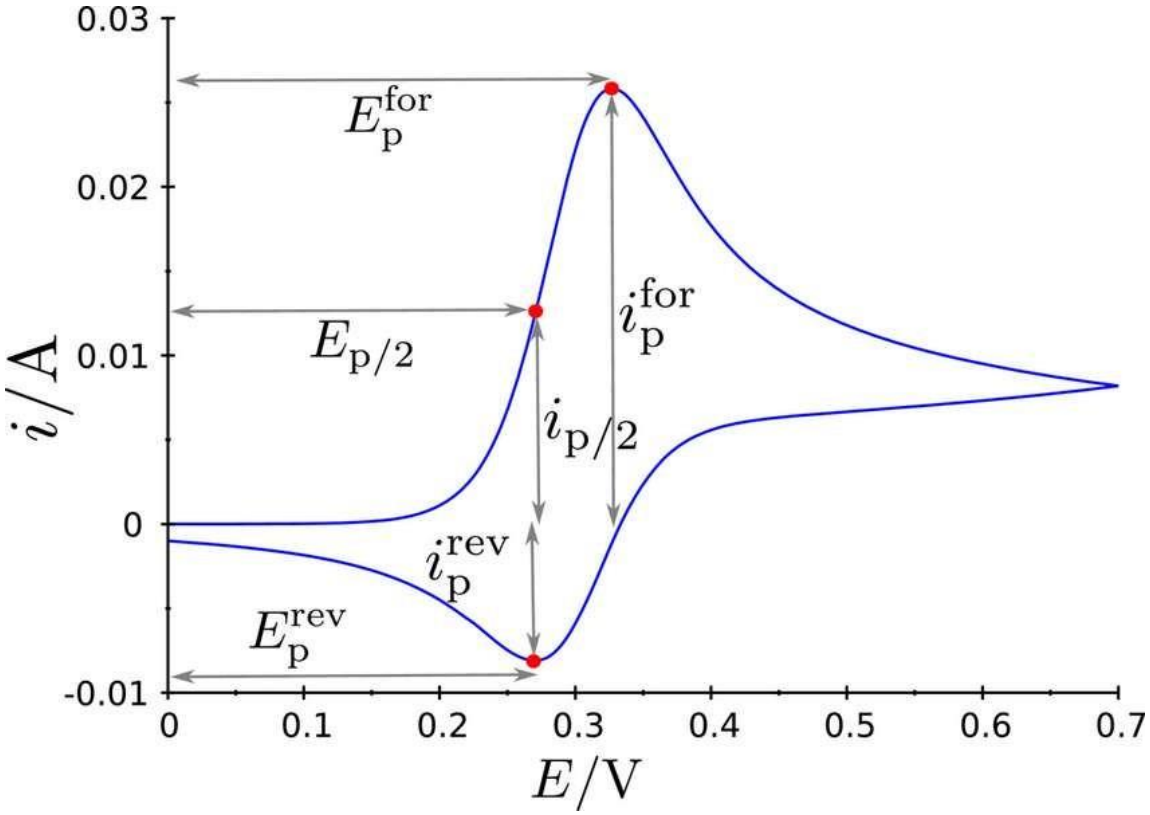

Figure 3.5. CV profile [7].

3.5.2 Chronopotentiometry

Chronopotentiometry is an electrochemical analysis method where the electrodes are subjected to a constant flow of current in order to the cause a constant reduction of the electroactive material Figure 3.7. This method is differentiated from constant-current coulometric analysis and coulometric titrimetry1 because in this technique the applied current appears to be significantly large so that the efficiency of current required for the reduction of the material is reduced below 100% within a few seconds.

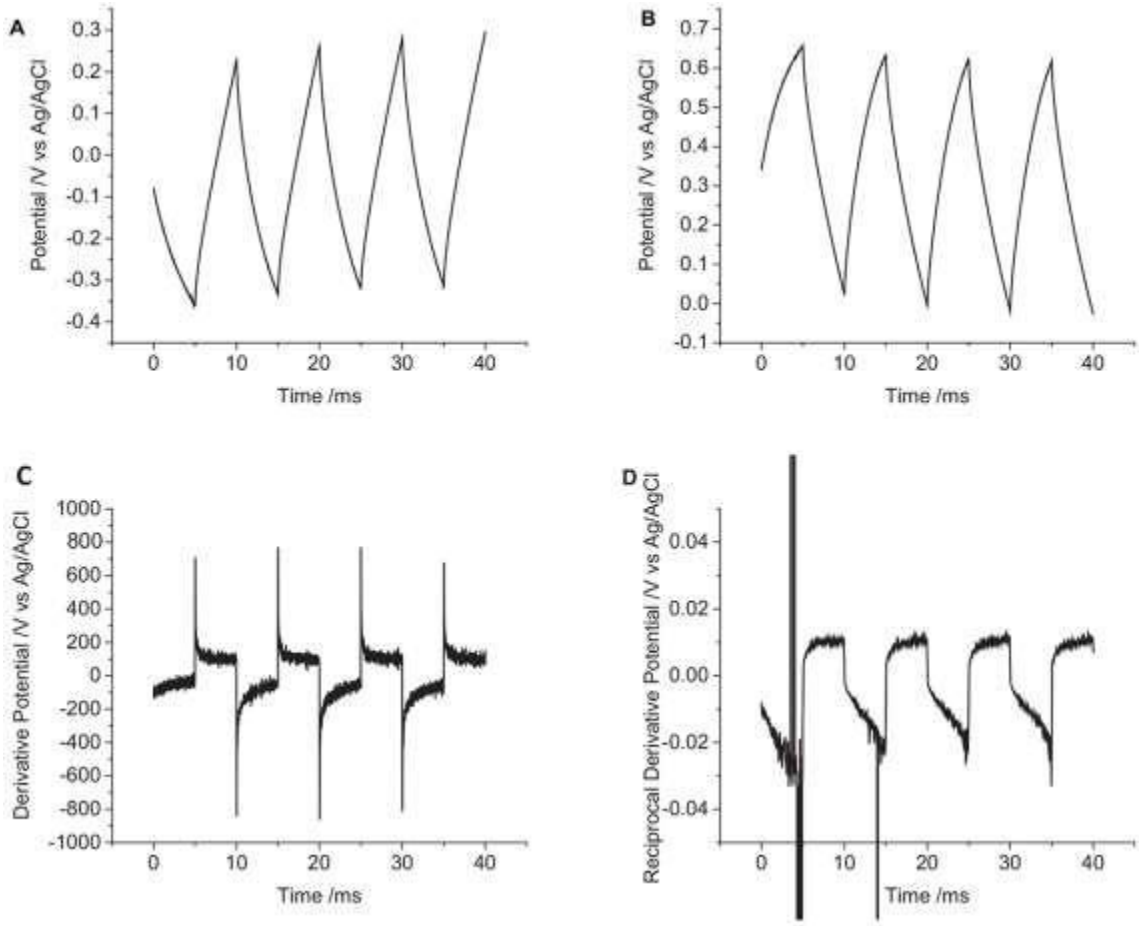

Figure 3-6. Chronopotentiometry Profile [8].

3.5.3 Electrochemical Impedance Spectroscopy (EIS)

This technique of electrochemical workstation allows us to measure the resistivity of our system. This includes resistance of electrolyte, ohmic loss and or activation losses. Electrical resistance is the measure of the of a circuit element that resists current flow.

$$R = E/I \quad (3)$$

According to Ohm's law, R is the resistance which is defined as the ratio of voltage (E), and current (I). This known law use is limited to only one circuit element, the ideal resistor. An ideal resistor has several simplifying properties:

- Ohm's Law is followed at every range of current and voltage.
- Resistance is not dependent on the frequency.
- The voltage passing through a resistor and the AC current are in a single phase.

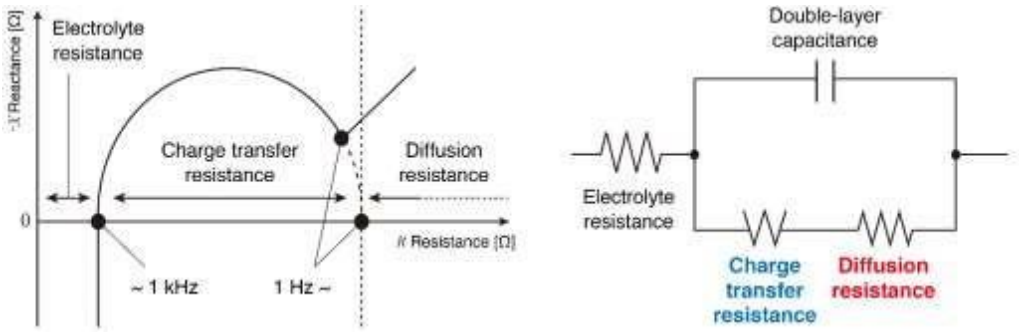

Figure 3.7. EIS Profile (Nyquist Plot) [9].

3.6 Electrochemical Parameters

The determination of the energy density and power density is very important to evaluate the efficiency of a supercapacitor for real-life applications. Cyclic voltammetry (CV) and chronopotentiometry are the techniques that can confirm the energy and power densities by using the following equations:

The specific capacitance (C, Fg^{-1}) can be determined using cyclic voltammetry:

$$C_s = \frac{\int IdV}{2mv\Delta V} \tag{4}$$

Here, ∫IdV is the integral area of the CV curves, m represents the mass, n represents the scan rate used to perform the analysis, and the voltage window of the process is represented by V.

$$E = \frac{1}{2}\frac{C_m \Delta V^2}{3.6} \tag{5}$$

Here, E is the symbol for energy density. The specific power (W/kg) defines how rapidly a device is able to deliver energy under a constant current density to external loads. The maximum specific power is calculated as:

$$P = \frac{E}{\Delta t} \times 3600 \tag{6}$$

Here, P represents the maximum power that can be achieved by a supercapacitor.

Summary

This chapter initially discusses different chemical synthesis methods like solvothermal and hydrothermal method. After that material characterization techniques have been studied i.e., XRD, SEM, EDS, TGA, BET and XPS . Main principle of these techniques has been noted down along with diagrams. After that the whole electrochemical testing process implemented was explained including ink formation, ink deposition on substrate and electrochemical performance determination using various techniques like CV, CP, and EIS with a three-electrode system.

List of References

[1] T. Takahashi, K. Kuwabara, and M. Shibata, “Solid-state ionics - conductivities of Na+ ion conductors based on NASICON,” *Solid State Ionics*, vol. 1, no. 3–4, pp. 163–175, 1980, doi: 10.1016/0167-2738(80)90001-6.

[2] N. S. Mohamed, R. H. Y. Subban, and R. Rusdi, “Enhancement of electrical properties of NASICON-type solid electrolytes (LiSn2P3O12) via aluminium substitution,” *J. Sci. Adv. Mater. Devices*, vol. 5, no. 3, pp. 368–377, 2020, doi: 10.1016/j.jsamd.2020.06.003.

[3] F. Zheng, M. Kotobuki, S. Song, M. O. Lai, and L. Lu, “Review on solid electrolytes for all-solid-state lithium-ion batteries,” *J. Power Sources*, vol. 389, no. April, pp. 198–213, 2018, doi: 10.1016/j.jpowsour.2018.04.022.

[4] C.J.Brinker;G.W.Scherer,“Sol-Gel_Science_The_physics_and_chemistry_of_sol-gel_processing_-_Brinker_1990.pdf.” p. 462, 1990. doi: 10.1016/S0254-0584(02)00315-2.

[5] S. D. Lee *et al.*, “Composite Electrolyte for All-Solid-State Lithium Batteries: Low-Temperature Fabrication and Conductivity Enhancement,” *ChemSusChem*, vol. 10, no. 10, pp. 2175–2181, 2017, doi: 10.1002/cssc.201700104.

[6] J. Lai, W. Niu, R. Luque, and G. Xu, “Solvothermal synthesis of metal nanocrystals and their applications,” *Nano Today*, vol. 10, no. 2, pp. 240–267, 2015, doi: 10.1016/j.nantod.2015.03.001.

[7] X. Dong, M. Qi, Y. Tong, and F. Ye, “Solvothermal synthesis of single-crystalline hexagonal cobalt nanofibers with high coercivity,” *Mater. Lett.*, vol. 128, pp. 39–41, 2014, doi: 10.1016/j.matlet.2014.04.133.

[8] S. Sōmiya and R. Roy, “Hydrothermal synthesis of fine oxide powders,” *Bull. Mater. Sci.*, vol. 23, no. 6, pp. 453–460, 2000, doi: 10.1007/BF02903883.

[9] S. Feng and R. Xu, “New materials in hydrothermal synthesis,” *Acc. Chem. Res.*, vol. 34, no. 3, pp. 239–247, 2001, doi: 10.1021/ar0000105.

Chapter 4: Methodology and Experimentation

4.1 Chemical Reagents

Cobalt Nitrate hexahydrate ($Co(NO_3)_2 \cdot 6H_2O$) (99%), 2–Methyl imidazole (99.8%), Selenium powder (99.5%), Methanol (99.8%) and Ethanol (99.8%). All the chemicals are of analytical grade, purchased from Sigma Aldrich/Alfa Aesar/Analar.

4.2Material Synthesis

4.2.1 Synthesis of ZIF-67

ZIF 67 framework was synthesized through a co-precipitation method. In general synthesis, ZIF-67 was synthesized by adding 1.436g of cobalt nitrate hexahydrate ($Co(NO_3)_2 . 6H_2O$) in 25ml of methanol, stirring it for 30 minutes till all $Co(NO_3)_2.6H_2O$ got fully dissolved. Similarly, 3.244g of 2-methylimidazole was dissolved in 25 ml of methanol until a clear solution of 2-methyl imidazole was formed [1]. Later, the Cobalt nitrate solution was added into 2-methyl imidazole solution with continuous stirring for 2 hours and then aged for 24 hours. After 24 hours, the resulting mixture was centrifuged, and purple precipitates were collected at the end, washed with methanol multiple times then dried at 80°C for 12 hours.

4.2.2 Preparation of CoSe/NC

The as-synthesized ZIF-67 was grounded with selenium powder, keeping the mass ratio of ZIF-67 to selenium as (1g:0.2g), (1g:0.6g), and (1g:1g) named as CoSe-0.2, CoSe-0.6 and CoSe-1 respectively. Here, ZIF-67 mass is kept fixed in all three samples. These grounded samples were then pyrolysed under Ar/H_2 atmosphere in a ceramic boat, heated to 800° C for 4 hours, the ramp rate was 5° C min−1. The black pyrolyzed material so obtained was finely grounded and then proceeded for further testing.

4.3 Material Characterization

XRD analysis was done on (D8 Advance by Bruker Germany with Cu K radiation (λ=0.154nm) with a 2θ range of 0° to 80°, while SEM analysis was performed on

(TESCAN MIRA3, model 51-sADD0007) with EDS to find out the morphologies of as synthesized composites. TGA analysis was done on TGA (Shimadzu DTG 60-H) in inert atmosphere (Nitrogen gas) in a temperature range of 20° C to 800° C at a ramp rate of 5° C/min. Confirmation of D and G bands were done by doing RAMAN technique on RAMAN (BWTEK, BAC 102-532).

4.4 Electrochemical Measurements

Electrochemical workstation 660E by CH instruments was used to execute the electrochemical testing of the prepared electrodes. Cyclic voltammetry (CV), gravimetric charge-discharge (GCD), and electrochemical impedance spectroscopy (EIS) were carried out in three electrode configurations. In this three-electrode system, Ag/AgCl was used as reference electrode, with platinum wire as counter electrode, while glassy carbon was used as current collector. 3 M KOH was used as aqueous electrolyte for the testing. The slurry was prepared by adding 2 mg active material, 20 µl binder (Nafion perfluorinated resin solution, 5%), and 80 µl ethanol, after mixing this mixture was sonicated for 30 minutes to obtain a homogeneous slurry. A drop of 1.5 µl was casted on glassy carbon with the help of micropipette and dried for 5-10 minutes at room temperature to make working electrode. The potential window of 0V – 0.5V was selected to perform electrochemical testing for the KOH electrolyte.

Summary

This chapter includes the total experimentation that was involved in the research process. The synthesis process of ZIF-67, selenization of ZIF-67 to form CoSe/NC composites along with their characterization techniques used were thoroughly demonstrated in the chapter. Finally, the electrochemical testing techniques which were used on electrochemical workstation and the testing parameters are discussed.

List of References

[1] W. Yang, X. Shi, Y. Li, H. Pang, Manganese-doped cobalt zeolitic imidazolate framework with highly enhanced performance for supercapacitor, J. Energy Storage. 26 (2019) 1–7. https://doi.org/10.1016/j.est.2019.101018.

Chapter 5: Results and Discussion

5.1 Material Characterization

5.1.1 X-ray Diffraction (XRD)

Fig 5(a) shows XRD of ZIF 67. The XRD diffraction peaks matched exactly with the previous literature [39] showing successful formation of ZIF-67. Fig 1(b) shows the XRD of CoSe/NC composites as given in JCPDS card number (70-2870), the peaks corresponding to the crystallographic plane values such as (101), (102), (110), (103), (201), (202), centered at 2θ values of 33.28°,44.92°,50.71°,60.34°,62.26°,70.4° respectively, all peaks being assigned to CoSe, hexagonal in structure [40].If we compare the XRD diffraction patterns of three as synthesized CoSe composites it can be clearly seen that as we increase the mass ratio of selenium powder from (0.2 to 1g) the intensity of peaks also increases depicting the increase in the crystallinity of CoSe composites[41]. In case of (CoSe-1) the diffraction peak at 50.71° is a bit sharper as compared to (CoSe-0.6 and CoSe-0.2) because in this sample the selenium powder is present in its maximum amount (ZIF-67 and selenium powder are present in equal mass ratio) leading to increase in crystallinity of CoSe at (110) crystallographic plane. Since the peaks are not highly intense, showing that the carbonized material has more defects and is more porous in nature, also there is no peak of carbon in XRD which could be linked with the degree of graphitization or carbon content in these composites None of the impurity peaks are observed in XRD, showing the successful formation of CoSe/NC composites [38].

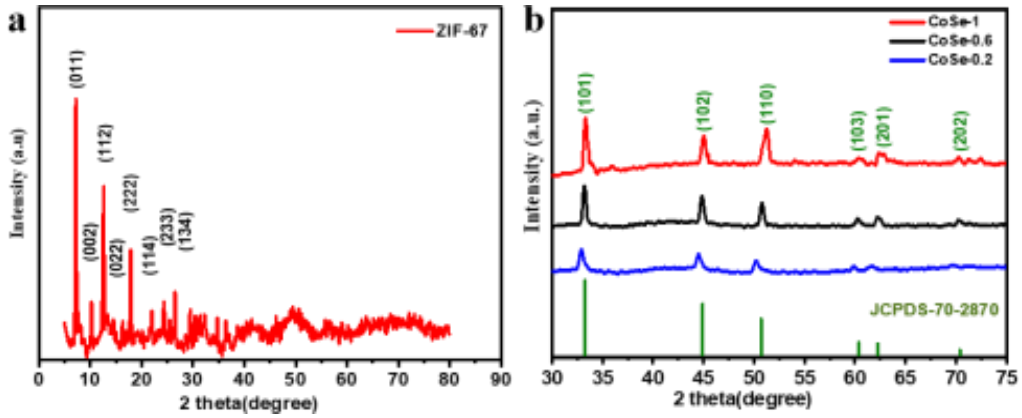

Figure 5.1. (a) XRD pattern (a) of ZIF-67 (b) CoSe-0.2, CoSe-0.6, CoSe-1

5.2 Scanning Electron Microscopy (SEM)

The structural morphology of as synthesized CoSe/NC composites were studied from SEM.SEM images were taken at a scale a range of 5μm. Fig. 5.1 (a) shows ZIF-67 being synthesized by co-precipitation method showed a distinct polyhedron morphology with a surface quite clear and smooth [42]. The structure of as synthesized ZIF-67 appeared rhombic dodecahedral structure matched exactly with structure of ZIF-67 reported in previously reported literature, since ZIF-67 polyhedron had clear surface means the as synthesized ZIF-67 were of pure quality. Well defined edges, side length were clearly confirming crystallographic features of ZIF-67 crystals. Fig. 5.1(b) shows surface morphology of ZIF-67 (pyrolysed in Ar/H_2 atmosphere) had a rough irregular morphology because it was annealed at 800 °C resulting in destruction of polyhedron rhombic crystals of ZIF-67. Fig. 5.1(b, c, d) shows structural morphologies of CoSe-0.2 ,CoSe-0.6 and CoSe-1.It can be clearly seen that by increasing the amount of selenium the distorted polyhedron structure of ZIF-67 had become more and more rough, nanoporous carbon formation on the surface also increased with increasing the amount of selenium[41]. Fig.5.1(f) shows EDS spectrum of CoSe-1. Table 1 shows presence of cobalt, Selenium, Nitrogen, Oxygen in as synthesized Cobalt selenide composites confirming the presence of basic essential elements in the as synthesized composites.

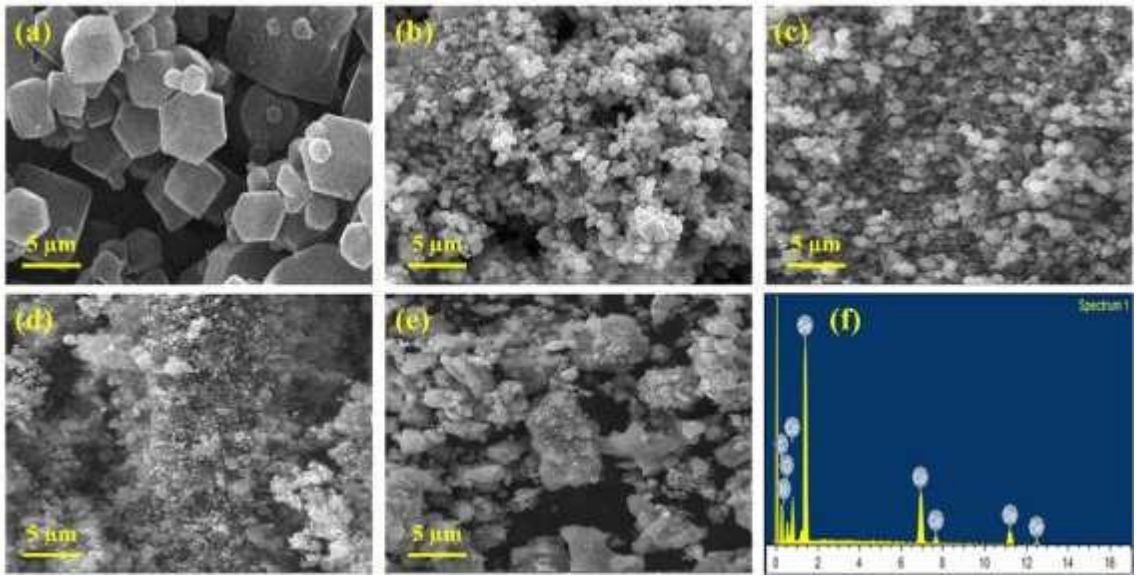

Figure 5.2. SEM images of (a) ZIF-67 before pyrolysis(b) ZIF-67 after pyrolysis (c) CoSe-0.2 (d)CoSe-0.6 (e)CoSe-1 (f) EDS spectrum of CoSe-1

Table 5.1

Elemental analysis of synthesized electrodes

Sample	Co(wt%)	Se(wt%)	N(wt%)	C(wt%)	O(wt%)
CoSe-0.2	17.94	19.77	3.01	44.30	14.9
CoSe-0.6	21.08	34.87	2.03	34.65	7.36
CoSe-1	22.34	33.78	3.49	31.39	9.00

5.3 RAMAN Spectroscopy

RAMAN Spectroscopy was conducted in order to affirm the presence of carbon content in as synthesized CoSe/NC composites. In Fig 5.3. two broad peaks can be clearly observedat 1348cm^{-1} and 1580cm^{-1}, which can be assigned as D bands (A_1g mode) shows defectsor amorphous carbon defects while G bands (E_2g mode) shows Graphitic carbon band depicting the presence of carbon in CoSe/NC composites [43].The resulting value of I_D/I_G ratio between the D and G bands can be used to find extent of graphitization with alesser value of I_D/I_G shows more extent of graphitization. Here in this case I_D/I_G ratio is 0.90 showing that the material has more carbon defects because the material was pyrolysed at higher temperature i.e. 800 °C [44].

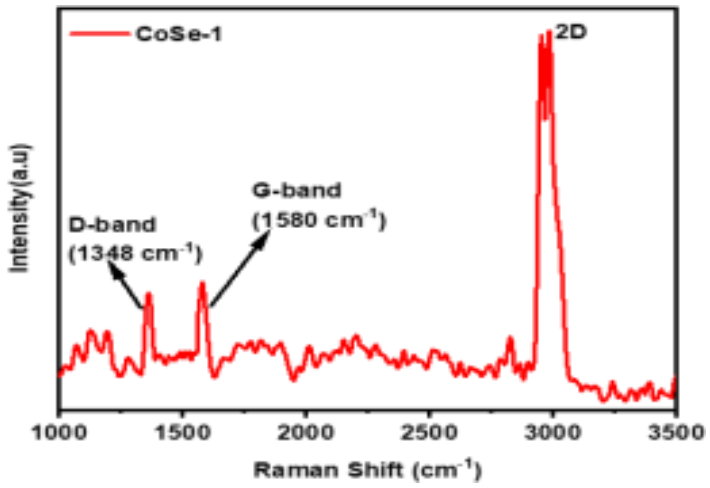

Figure 5.3. RAMAN spectra of CoSe-1

5.4 Thermogravimetric Analysis

TGA analysis was done for CoSe-1 in an inert environment (N_2 atmosphere) at 800° C. The mass loss till 350° C could be due to removal of water content from the CoSe-1.Afterwards, there is quick mass loss of about 21% that could be because of chemical reaction between selenium powder and ZIF-67[40] .Then there will be further decrease in mass loss because of degradation and carbonization of organic ligands of ZIF-67.The actual degradation of ZIF-67 occurs at nearly 600° C[45] .A breakage of chemical linkage between Cobalt and constituent organic ligands in ZIF-67 results in a chemical bonding between Selenium and cobalt and the left over organic frameworks kept on degrading around 600°C. 10% weight loss after 600°C due to mutual effect of selenium evaporation along with carbonization of organic species in the material. In Fig. 3 we can see there is gradual increase in mass loss till 800° C, it becomes stable after 800° C as reported in previous literature[40] showing pyrolysis temperature should be greater than 800° C for absolute carbonization of organic constituents.

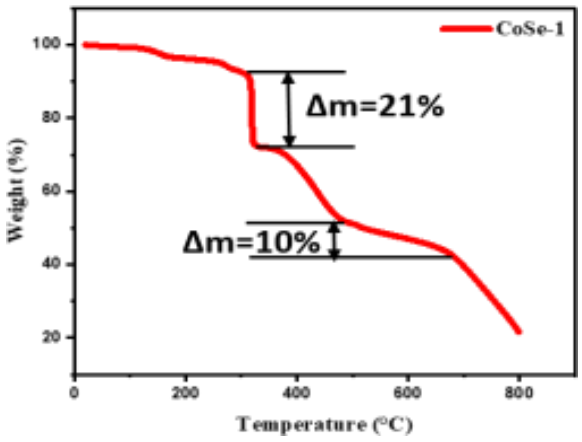

Figure 5.4. TGA profile of CoSe-1 at 800 °C in N_2 atmosphere

5.5 Brunauer-Emmett-Teller (BET)

Figure 5.5 (a) exhibits the N_2 adsorption desorption of all the prepared electrodes i.e CoSe-0.2,CoSe-0.6, CoSe-1, all the samples showing type IV type isotherm with the hysteresis loop exist in a region of 0.4 to 1 relative pressure of N_2 , materials with mesoporous structure generally shows type IV isotherms.Figure5.5(b) shows

BJH pore size distribution of all the prepared samples, depicting that average pore size lies in the region of 2 to 10 nm while some particles lies in the microporous region that can be clearly seen from graph(b).

Table 5.2 *Comparison of Pore size, pore volume and surface area*

Sample	Multipoint BET surface area (m^2g^{-1})	Pore radius (nm)	Pore volume (cm^3g^{-1})
CoSe-0.2	175.02	1.82	0.287
CoSe-0.6	153.01	1.81	0.181
CoSe-1	75.69	1.80	0.15

If we see surface area of all samples , it can be seen that by increasing amount of selenium, surface area is increasing, CoSe-1 has shown maximum surface area which is the reason for maximum specific capacitance of CoSe-1 Sample.

5.2 Electrochemical Performance

The electrochemical performance of the material was evaluated using CV, GCD, and EISin a 3-electrode system.

5.2.1 Cyclic Voltammetry (CV).

The electrochemical behaviour of as prepared electrodes were examined by Cyclic Voltammetry ,Chronopotentiometry, Electrochemical Impedance Spectroscopy in 3M KOH solution.CV curves were analysed at different scan rates 2, 3 ,5 10, 20, 40, 50 mV s^{-1}

1 within a potential range of 0-0.5V.Fig.5.5(a) shows CV profile of Pyrolysed ZIF-67 at above mentioned sweep rates.Its CV curves shows supercapacitor behaviour of the synthesized electrode.Fig.5.5(b) shows CV profiles of CoSe-0.2,its CV curves also showing that the as prepared electrode has a supercapacitor like behaviour. Fig. 5.5(c) shows CV curves of CoSe-0.6, exhibiting pseudo capacitor behaviour of the electrodes, itis showing anodic peaks and cathodic peaks at 0.22V and 0.18V. Fig 5.5(d) shows CV profiles CoSe-1, it can be seen that anodic peaks appear at 0.32V at $2mVs^{-1}$ this anodic peak further shifts to 0.29 V at $3mVs^{-1}$,these peaks got disappeared at higher scan rates,showing pseudo capacitor like behavior of the prepared electrode. Fig 5.5(e) analogy CV curves at same sweep rate i.e $5mVs^{-1}$,the area of CV profiles is directly linked with the sweep rates .The cathodic and anodic peaks can be linked with insertion of electrolyte ion within the electrode material layered structure resulting because of ongoing electrochemical reaction and reversible change of oxidation state of Cobalt ions. If we increase selenium amount further by keeping ZIF-67 amount constant (1g :1.4g), named as CoSe-1.4 there will be sharp decrease in specific capacitance value i.e 197F g-1 at 2mVs-1 (Electrochemical results and XRD pattern are shown in supplementary data (S1)).

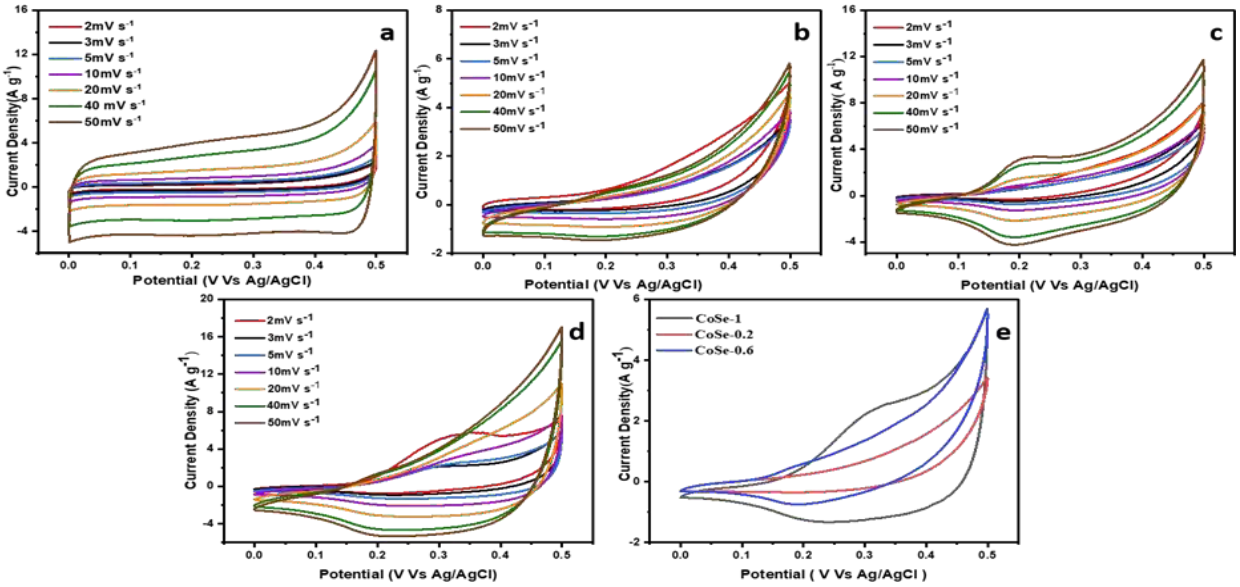

Fig. 5-5. CV curves of (a) Pyrolysed ZIF-67(b) CoSe-0.2 (c) CoSe-0.6(d) CoSe-1 (e)sComparsion of CV curves of CoSe-0.2, CoSe-0.6,CoSe-1 at 5mV s-1

Specific Capacitances are calculated from CV curves showing using formula[46]

$$C_s = \frac{Q}{2\,\Delta V m} \quad (1)$$

where m depicts mass loading of the on working electrode (i.e. glassy carbon) while ΔV represents voltage window difference,Q is the average integral area of CV curve.

According to this, CoSe-1 showed a highest specific capacitance of 746F g^{-1} at 2mVs^{-1} whereas CoSe-0.2 and CoSe-0.6 showed specific capacitances of 278 F g^{-1} and 483F g^{-1} at 2mVs^{-1} respectively. This could be related to amount of selenium in the electrode material CoSe-1 having maximum amount of selenium while CoSe-0.2 has least amount of selenium powder. Pyrolysed ZIF-67 showed a capacitance of 131F g^{-1}. Table 5.2 is showing the capacitances of all electrode materials at different scan rates. It can be observed that specific capacitance value drops as we move from lower to higher scan rates This can be justified by two possibilities /conditions. At low sweep rates, kinetic energy of ions is low thereby offering lower resistance, providing more time for electrolyte ions to interact with porous electrode material causing an increase in specific capacitance values. At faster scan rates kinetic energy of electrolyte ions is more, causing hindrance in electrolyte adsorption on porous electrode material surface thereby allowing less time for electrolyte ions to interact with electrode material surface causing a decrease in values of specific capacitances

Table 5.3 *Sweep rates versus specific capacitances of electrode material*

Sweep Rate (mV s^{-1})	**Specific Capacitances (F $g^{-1)}$**			
	Pyrolysed ZIF-67	**CoSe-0.2**	**CoSe-0.6**	**CoSe-1**
2	131	278	483	746
3	113	106	260	301
5	100	71	190	229
10	91	49	143	165
20	83	33	111	118
40	77	22	86	81
50	22	20	81	71

5.2.2 Capacitive and Diffusive Contribution

A comprehensive mathematical analysis was carried out to gain a deeper insight into the material charge storage behavior. The electrode material's total specific capacitance can be split into two components based on the storage mechanism: EDLC and diffusion. EDLC is attributed to the surface adsorption and desorption of ions and is rapid and unassociated with the scan rate. On the other hand, diffusion control is dependent on the electrolyte ions' diffusion into the electrode material's surface. To reach conclusive outcomes, it is essential to determine which process dominates during an electrochemical reaction. The capacitive and diffusive behavior of electrode samples were found out by equation (2) [13]in order to understand the charge storage procedure by Dunn's method[47] . For a linear scan rate, the current is given by Equation 5.

$$i = av^b \tag{5}$$

Where *i* represents current, *v* represents voltage, and *a* and *b* are constants. The value of *b* is equal to 1 for the EDLC process and 0.5 in the case of diffusion controlled. In most cases, the value of *b* remains between 0.5 and 1. Rearranging Equation 1 as:

$$i(V) = k_1 v + k_2 v^{1/2} \tag{6}$$

Where *i(V)* is the value of the current at a fixed potential. The constants k_1 and k_2 are given by the slope and intercept of a linear regression plot between current and $v^{1/2}$, respectively. This equation shows that the current (i) is sum of total capacitive current (k1v) and diffusive current(k2v1/2). k1 is constant that gives capacitive current while k2 constant gives diffusive current. k1 shows slope while k2 shows intercept of linear graph plot between i/v1/2 and v1/2 respectively. Fig 5.6. shows capacitive current depends on scan rate, showing that the capacitive behavior is more dominant while capacitive behavior gets masked at higher scan rates.CoSe-1 is showing maximum surface capacitive current as compared to CoSe-0.6,CoSe-0.2 at 50mV s^{-1} as shown in Fig 5.6.

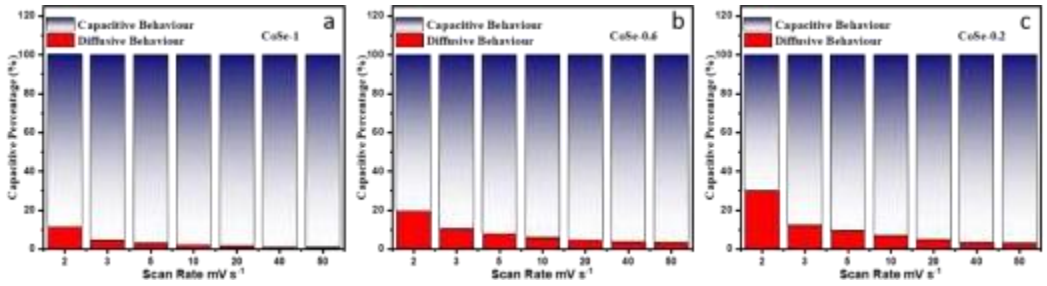

Figure 5.6. Capacitive and Diffusive behavior of (a) CoSe-1 (b) CoSe-0.6 (c) CoSe-0.2

5.2.3 Chronopotentiometry

iChronopotentiometry technique was done to understand the charge discharge behavior of all the electrode materials. GCD technique was performed at different values of current densities like at 0.5, 0.7, 1, 2, 3, 4 A $g^{-1.}$ Fig .7 shows the GCD profiles of (a) pyrolysed ZIF-67 (b) CoSe-0.2 (c) CoSe-0.6. It is evident from Fig 5.7 that GCD curves of pyrolysed ZIF-67, CoSe-0.2 and CoSe-1 has almost linear shape showing EDLC like behavior, which could be linked with good electrochemical reversibility of electrode material while in case of CoSe-0.6, hump at 0.18V showing the faradic reaction occurring on the surface of electrode material, matches exactly with its CV curve. Fig 5.7(e) shows analogy of GCD curves at a current density of 1A g^{-1}.

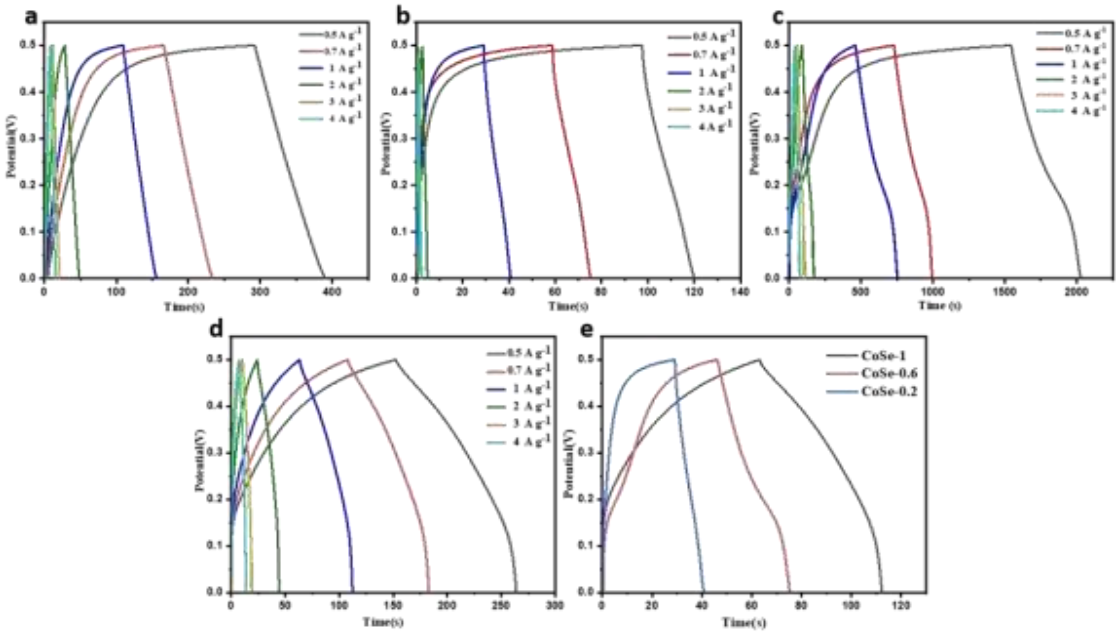

Fig 5.7. GCD profiles of (a) pyrolysed ZIF-67 (b) CoSe-0.2 (c) CoSe-0.6 (d) CoSe-1 (e)Comparison of GCD curves of b, c, d at 1 A g^{-1}.

5.2.4 Electrochemical Impedance Spectroscopy

In order to examine the charge storage process and resistance offered to conductivity and charge transfer of electrode material, EIS was performed in a frequency range of 1Hzto 100kHz.The equivalent circuit is also shown in Fig 8. An ideal super capacitor shows larger slope value in lower frequency region near to Y-axis while the semi-circle diameter should be smaller [48, 49].Semi circle in medium to higher frequency region shows the Rct (charge transfer resistance while the slope line is exhibiting Warburg resistance (Rw)[50]. Rct of all 3 electrode materials CoSe-0.2, CoSe-0.6, CoSe-1 from the equivalentcircuit were found to be 9.56 ,9.5 ,1 Ω. It can be clearly seen that in case of CoSe-1, the semicircle arc has shorter diameter than in case of CoSe-0.6 and CoSe-0.2 also it has greater slope in lower frequency region. Also, the Rct value is lowest in case of CoSe-1,
in comparative to CoSe-0.6and CoSe-0.2 exhibiting faster charge transfer, enhancing the circulation of electron with porous electrode samples leading to an increase in electronic conductivity hence specific capacitance of as synthesized electrode materials. Rct value is maximum in case of CoSe-0.2 as it has greater semicircle arc diameter as compared to CoSe-0.2 and CoSe-1. Also the solution resistance (Rs) value is also lowest in case of CoSe-1 i.e 5.1 Ω therefore the electrode material exhibited highest capacitance value while Rs in case of CoSe-0.2 and CoSe-0.6 is 5.9 Ω and 5.2 Ω respectively. Table 3 shows the Rct, Rs and specific capacitances of all the three electrode material.

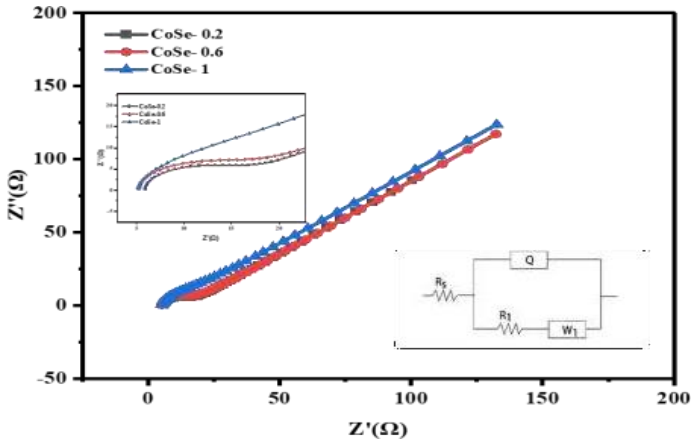

Fig 5.8 Nyquist plot of CoSe-0.2, CoSe-0.6, CoSe-1

Table. 5.4 *Specific capacitances, Rs and Rct of CoSe-0.2, CoSe-0.6, CoSe-1*

Sample	Specific Capacitance(F/g)	Rs Ω	Rct Ω
CoSe-0.2	278	5.9	9.56
CoSe-0.6	483	5.2	9.5
CoSe-1	746	5.1	1

5.2.5 Cyclic stability

In order to check the electrochemical performance, cyclic stability of CoSe-1 was performed over 4000 cycles at a sweep rate of 100mVs^{-1}. Fig 5.9 depicts it has retained about **82.3% capacitance after 4000 cycles**. This could be because of the reason that electrode material is more porous having larger number of active sites leading to faster oxidation reduction reaction on surface of electrode and faster movement of electrolyte ion within the pores of N-doped Carbon based electrode material causing an increase in structural stability after repetitive cycling.

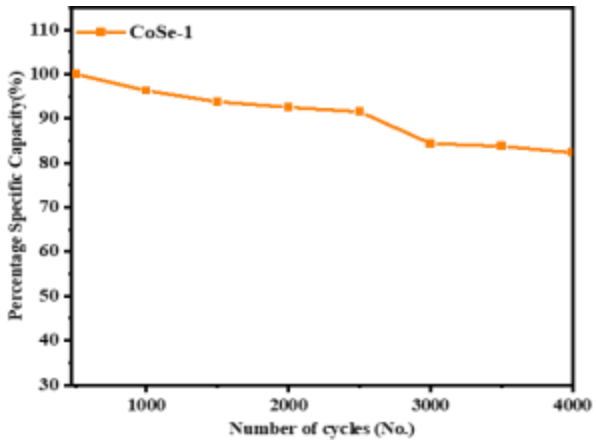

Fig 5.9. Cyclic Stability of CoSe-1 at 100mV s^{-1} for 4000 cycles.

Table 5.5. *Comparison of similar electrodes specific capacitance from literature*

Electrode	Electrolyte	Specific capacitance(F g^{-1})/Specific capacity(C g^{-1})	Cyclic Stability	Ref.
N dopedCoSe2/C	2M KOH	726 F g^{-1}	84.7% after 5000 cycles	[51]
$NiCoSe_2$	2M KOH	300.2F g^{-1}	100% after 2000 cycles	[41]
(Ni,Co)Se2	3M KOH	401.1 C g^{-1}	43.3% after 10000 cycles	[52]
CoSe thin films	0.1 KCl	510 F g^{-1}	91% after 5000 cycles	[53]
$Co_{0.85}Se$	2M KOH	31m A h g^{-1}	83% after 10,000 cycles	[54]
$CoSe_2$/NC	6 M KOH	120.2 m A h g^{-1}	92% after 10,000 cycles	[54]
CNT@$Co_{0.85}Se$	2 M KOH	638 F g^{-1}	97.3% after 5000 cycles	[55]
CoSe/NC composites	3M KOH	746 F g^{-1}	82.3% after 4000 cycles	This work

Conclusion

CoSe/NC composites (CoSe-0.2, CoSe-0.6, CoSe-1) were synthesized by taking ZIF-67 and selenium powder as precursor material, annealed in a reducing atmosphere (Ar /H_2) at 800° C.XRD analysis confirmed the formation of CoSe. Among all the three CoSe/NC composites, CoSe-1 exhibited best electrochemical behavior showing a specific capacitance value of 746 F g^{-1} at 2mV s^{-1}, because of the optimize ratio of cobalt and selenium in this composite material. Also, EIS of CoSe-1 shows the Rct value is 1.0 Ω, least value among all the CoSe/NC composites showing greater charge transfer hence leading to higher value of specific capacitance, with a cyclic stability of 82.3% after 4000 cycles, thereby showing it a good candidate to be used as electrode material in supercapacitors.

List of references

- Q. Yang, R. Lu, S. Ren, C. Chen, Z. Chen and X. Yang Chemical Engineering Journal 2018 Vol. 348 Pages 202-211
- Y. Zhang et al., "Nitrogen-doped yolk–shell-structured CoSe/C dodecahedra for high-performance sodium ion batteries," ACS applied materials & interfaces, vol. 9, no. 4, pp. 3624-3633, 2017.
- Z. Li, L. Y. Zhang, L. Zhang, J. Huang, and H. Liu, "ZIF-67-derived CoSe/NC composites as anode materials for lithium-ion batteries," Nanoscale Research Letters, vol. 14, pp. 1-11, 2019.
- Q. Wang et al., "ZIF-67 derived amorphous CoNi2S4 nanocages with nanosheet arrays on the shell for a high-performance asymmetric supercapacitor," ChemicalEngineering Journal, vol. 327, pp. 387-396, 2017.
- Y. Miao et al., "Polyhedral NiCoSe2 synthesized via selenization of metal-organicframework for supercapacitors," Materials Letters, vol. 242, pp. 42-46, 2019.
- R. Ahmad et al., "Zeolitic imidazolate frameworks derived Co-Zn-nanoporous carbon-sulfide material for supercapacitors," Electrochimica Acta, vol. 404, p. 139739, 2022.
- F. Zheng, Y. Yang, and Q. Chen, "High lithium anodic performance of highly nitrogen-doped porous carbon prepared from a metal-organic framework," Nature communications, vol. 5, no. 1, p. 5261, 2014.
- Y. Zhang et al., "Nitrogen-doped yolk–shell-structured CoSe/C dodecahedra for high-performance sodium ion batteries," ACS applied materials & interfaces, vol. 9, no. 4, pp. 3624-3633, 2017.
- X. Wang et al., "MOF derived catalysts for electrochemical oxygen reduction," Journal of Materials Chemistry A, vol. 2, no. 34, pp. 14064-14070, 2014.
- Y. Zhang et al., "Nitrogen-doped yolk–shell-structured CoSe/C dodecahedra for high-performance sodium ion batteries," ACS applied materials & interfaces, vol. 9, no. 4, pp. 3624-3633, 2017.

- J. Wang, J. Polleux, J. Lim, and B. Dunn, "Pseudocapacitive contributions to electrochemical energy storage in TiO2 (anatase) nanoparticles," The Journal of Physical Chemistry C, vol. 111, no. 40, pp. 14925-14931, 2007.
- J. Yang and S. Gunasekaran, "Electrochemically reduced graphene oxide sheets for use in high performance supercapacitors," Carbon, vol. 51, pp. 36-44, 2013.
- R. Wang et al., "Electrochemical properties of manganese ferrite-based supercapacitors in aqueous electrolyte: the effect of ionic radius," Colloids and Surfaces A: Physicochemical and Engineering Aspects, vol. 457, pp. 94-99, 2014.
- M. Itagaki, S. Suzuki, I. Shitanda, and K. Watanabe, "Electrochemical impedance and complex capacitance to interpret electrochemical capacitor," Electrochemistry, vol. 75, no. 8, pp. 649-655, 2007.
- Y. Zhang et al., "Self-templated synthesis of N-doped CoSe2/C double-shelled dodecahedra for high-performance supercapacitors," Energy Storage Materials, vol. 8, pp. 28-34, 2017.
- Y. Miao et al., "Polyhedral NiCoSe2 synthesized via selenization of metal-organicframework for supercapacitors," Materials Letters, vol. 242, pp. 42-46, 2019.
- H. Chen, W. Li, M. He, X. Chang, X. Zheng, and Z. Ren, "Vertically oriented carbon nanotube as a stable frame to support the Co0. 85Se nanoparticles for high performance supercapacitor electrode," Journal of Alloys and Compounds, vol. 855, p. 157506, 2021.
- Z. Qu, J. Li, M. Guo, L. Zhao, L. Duan, and S. Ding, "Design tremella-like Ni-Co selenide with wonderful electrochemical performances as supercapacitor cathode material," Electrochimica Acta, vol. 393, p. 139049, 2021.
- X. Zhang, J. Gong, K. Zhang, W. Zhu, J.-C. Li, and Q. Ding, "All-solid-state asymmetric supercapacitor based on porous cobalt selenide thin films," Journal of Alloys and Compounds, vol. 772, pp. 25-32, 2019.
- S. Wu et al., "One-pot synthesis of the flower-like Co0. 85Se nanosheets as an anode material for long-life aqueous asymmetric supercapacitor," Synthetic Metals, vol. 268, p. 116499, 2020.

- S. Wu et al., "One-pot synthesis of the flower-like Co0. 85Se nanosheets as an anode material for long-life aqueous asymmetric supercapacitor," Synthetic Metals, vol. 268, p.